

Tracking quintessence by cosmic shear

Constraints from VIRMOS-Descart and CFHTLS[★] and future prospects

Carlo Schimd^{1,2}, Ismael Tereno^{2,3}, Jean-Philippe Uzan², Yannick Mellier^{2,4},
Ludovic van Waerbeke⁵, Elisabetta Semboloni², Henk Hoekstra⁶, Liping Fu², and Alain Riazuelo²

¹ DSM/DAPNIA, CEA/Saclay, 91191 Gif sur Yvette cedex, France

² Institut d'Astrophysique de Paris, UMR7095 CNRS, Université Pierre & Marie Curie - Paris, 98 bis bd Arago, 75014 Paris, France

³ Departamento de Física, Universidade de Lisboa, 1749-016 Lisboa, Portugal

⁴ Observatoire de Paris - LERMA, 61 avenue de l'Observatoire, 75014 Paris, France

⁵ Department of Physics and Astronomy, University of British Columbia, 6224 Agricultural Road, Vancouver V6T 1Z1, Canada

⁶ Department of Physics and Astronomy, University of Victoria, Victoria V8P 52C, Canada

Received November 12, 2021; accepted ...

ABSTRACT

Context. Dark energy can be investigated in two complementary ways, by considering either general parameterizations or physically well-defined models. This article follows the second route and explores the observational constraints on quintessence models where the acceleration of our universe is driven by a slow-rolling scalar field. The analysis focuses on cosmic shear, combined with type Ia supernovae data and cosmic microwave background observations.

Aims. This article examines how weak lensing surveys can constrain dark energy, how they complement supernovae data to lift some degeneracies and addresses some issues regarding the limitations due to the lack of knowledge concerning the non-linear regime.

Methods. Using a Boltzmann code that includes quintessence models and the computation of weak lensing observables, we determine the shear power spectrum and several two-point statistics. The non-linear regime is described by two different mappings. The likelihood analysis is based on a grid method. The data include the “gold set” of supernovae Ia, the WMAP-1 year data and the VIRMOS-Descart and CFHTLS-deep and -wide data for weak lensing. This is the first analysis of high-energy motivated dark energy models that uses weak lensing data. We explore larger angular scales, using a synthetic realization of the complete CFHTLS-wide survey as well as next space-based missions surveys.

Results. Two classes of cosmological parameters are discussed: *i*) those accounting for quintessence affect mainly geometrical factors; *ii*) cosmological parameters specifying the primordial universe strongly depend on the description of the non-linear regime. This dependence is addressed using wide surveys, by discarding the smaller angular scales to reduce the dependence on the non-linear regime. Special care is paid to the comparison of these physical models with parameterizations of the equation of state. For a flat universe and a quintessence inverse power law potential with slope α , we obtain $\alpha < 1$ and $\Omega_{Q0} = 0.75^{+0.03}_{-0.04}$ at 95% confidence level, whereas $\alpha = 2^{+18}_{-2}$, $\Omega_{Q0} = 0.74^{+0.03}_{-0.05}$ when including supergravity corrections.

Key words. Gravitational lensing. Cosmology: theory – cosmological parameters. Methods – data analysis.

1. Introduction

Cosmological observations provide increasing compelling evidences that the expansion of the universe is accelerating and that the cosmic history of the universe seems today dominated by another component than its matter and radiation content (see e.g. Peebles & Ratra 2003; Carroll 2001; Padmanabhan 2003; Peter & Uzan 2005, chap. 12 for reviews and references therein). If so, one of the most challenging issue of fundamental physics is to understand the cause of this acceleration, a question often referred to as the nature of the *dark energy*. Various solutions, from the introduction of a new type of matter to a modification of general relativity to describe the

Send offprint requests to: carlo.schimd@cea.fr

[★] Based on observations obtained with MegaPrime/MegaCam, a joint project of CFHT and CEA/DAPNIA, at the Canada-France-Hawaii Telescope (CFHT) which is operated by the National Research Council (NRC) of Canada, the Institut National des Sciences de l'Univers of the Centre National de la Recherche Scientifique (CNRS) of France, and the University of Hawaii. This work is based in part on data products produced at TERAPIX and the Canadian Astronomy Data Centre as part of the Canada-France-Hawaii Telescope Legacy Survey, a collaborative project of NRC and CNRS.

gravitation interaction, have been considered. A classification of these models with some relevant observational tests that can help to distinguish between each class from their underlying new physics is discussed in Uzan (2004) and Uzan, Aghanim & Mellier (2004).

Dark energy appears in the Friedmann equations through its *effective* density and pressure. Data are usually interpreted assuming the validity of the Copernican principle (so that the dynamics of spacetime is completely described by a single function, the scale factor a) and the validity of Einstein equations (and thus the standard Friedmann equations), so that the density and pressure of the dark energy component are defined by $\rho_{\text{de}} = (3/8\pi G)(H^2 + K/a^2) - \rho_{\text{m}} - \rho_{\text{r}}$ and $P_{\text{de}} = (-1/8\pi G)(\ddot{a}/a + H^2 + K/a^2)$, where $H = \dot{a}/a$ is the Hubble parameter and a dot refers to a derivative with respect to the cosmic time, while ρ_{m} and ρ_{r} are the density of pressureless matter and radiation, respectively. It follows that the equation of state of the dark energy corresponds to

$$3\Omega_{\text{de}}w = -1 + \Omega_K + 2q, \quad (1)$$

where $q = -a\ddot{a}/\dot{a}^2$ is the deceleration parameter and $\Omega_K = -K/a^2H^2$. From this point of view, w characterizes the dynamics of the cosmic expansion. More precisely, it parameterizes the deviation, $H(z) - \bar{H}(z)$, between the Hubble function of the observed Universe, $H(z)$, and that predicted for a universe filled only with pressureless matter and radiation, $\bar{H}(z)$. It is therefore equivalent to specify $w(z)$ or $H(z) - \bar{H}(z)$. However, when general relativity is assumed to describe gravity, w reduces to $P_{\text{de}}/\rho_{\text{de}}$ so that, in addition to the deviation from $\bar{H}(z)$, it also gives some insight on the properties of dark energy (see e.g. Martin, Schmid & Uzan (2005) for a case in which w does not reduce to the equation of state of a matter component).

Although effective equation of state derived from observations is a key empirical information on the rough nature of dark energy, a detailed description of its properties demands more thoughtful data interpretation. For example, all geometrical observables rely on the integration of the Hubble parameter, hence on a double integration of the equation of state w , that eventually dilutes or totally washes out its possible redshift dependence. If w is close to -1 , as observations tend to indicate, then it is in general difficult to demonstrate by geometrical tests that $w \neq -1$ or that $dw/dz \neq 0$; both would exclude a pure cosmological constant. Exploring early properties of dark energy models would be even more challenging since for $w \simeq -1$ the ratio between the matter and dark energy densities scales approximately as $(1+z)^3$ so that dark energy is dynamically negligible at redshift $z \gtrsim 2$. It leaves little freedom to determine the scaling of the dark energy density and to demonstrate that it is not properly described by a power law $[(1+z)^n]$, as would be the case for a constant w (see e.g. Kujat et al. 2002).

From the theoretical point of view two routes can be followed. One can either exhibit a general “model-independent” parameterization of the equation of state of the dark energy, as discussed in the previous paragraph, or rely on a completely specified theoretical models. A useful parameterization has to be realistic, in the sense that it should reproduce predictions of a large class of models, it has to minimize the number of free parameters and to be simply related to the underlying

physics (see e.g. Linder & Huterer 2005). Because the result of the analysis will necessarily have some amount of parameterization dependence (Basset et al. 2002), choosing the specified physical model strategy seems preferable to break degeneracies. In particular, it enables to compute without any ambiguity their signature both in low and high redshift surveys, such as the cosmic microwave background (CMB). The increasingly flourishing number of models hampers to provide a comprehensive set of unambiguous predictions to constrain physical models one by one with present-day observations, but there are still several benefits in exploring dark energy this way, in particular when weak lensing surveys are used together with CMB observations. This is deeply related to the evolution of dark energy properties and the growth rate of structure with look-back time, as discussed below.

At low redshift, w suffices to get observable that are all functions of $H(z)$ (see for example Peebles 1993; Peter & Uzan 2005). This is the case of all background quantities (e.g. luminosity distance, angular distance, look-back time, etc.) as well as of the linear growth factor of density perturbations. It follows that the equation of state encodes all relevant information, provided the amplitude of the power spectrum is calibrated by adding a new parameter, σ_8 , the variance of the density perturbation on a scale of $8h^{-1}$ Mpc (see e.g. Benabed & Bernardeau 2001; Benabed & van Waerbeke 2003; Doran et al. 2000). However, as far as weak lensing is concerned, it was shown (Benabed & van Waerbeke 2003; Benabed & Bernardeau 2001) that, for a fixed redshift of the sources, the modification of the growth factor in the linear regime was degenerate with the normalization factor. Hence normalizing on the CMB avoids this problem, and at the same time it is important to describe the non-linear regime. The use of CMB together with weak lensing data is therefore a logical way to constrain specified theoretical models, beyond the description by an empirical equation of state.

At higher redshift, and in particular to relate the amplitude of the matter density power spectrum to the one of the primordial power spectrum, one would need to include a description of the evolution of the perturbations of dark energy. In particular, this effect becomes increasingly important as w approaches zero (Benabed & Bernardeau 2001). Note that dark energy perturbations have a non-adiabatic component that also requires a detailed model to be described. This depends on the physical model of dark energy and cannot be incorporated in a simple model-independent way.

While the ability of lensing data to constrain the equation of state of dark energy has been widely studied (Benabed & van Waerbeke 2003; Hu & Jain 2004; Jain & Taylor 2003), there have been very few analysis with real data. Hoekstra et al. (2005) and Semboloni et al. (2005) used the CFHTLS wide and deep data to constrain a constant equation of state. Jarvis et al. (2005) analyzed the 75 square degrees CTIO lensing survey, combined with type Ia supernovae (Sn Ia) data and CMB, assuming a constant equation of state and a parameterization of the form proposed by Chevallier & Polarski (2001) and then by Linder (2003). In this article, we consider a class of completely defined

quintessence models, realized by a self-interacting scalar field. Hence all observational signatures (Sn Ia, lensing, CMB) can be explicitly computed, with no ambiguity in the way to deal with the perturbations of dark energy. This theoretical extension of the standard Λ CDM model involves only one additional parameter, needed to characterize the self-interacting potential of the quintessence field. It follows that, as discussed above, we will be able to normalize our initial power spectrum on the CMB angular power spectrum and, as a consequence, σ_8 and any possible dependence on the shape of the analytical fit of the transfer function will disappear from our discussion; the value of σ_8 will be an output of each models. The problem of the pivot redshift (see § 2.2) that appears when combining different datasets also disappear in that approach. As a conclusion, this approach is very efficient in terms of the number of extra-parameters and of the interpretation of the data. Let us emphasize that, even though we also consider Sn Ia and CMB data, we will focus on weak lensing - cosmic shear data. This article, being the first analysis of the CFHTLS data for dark energy studies, illustrates the power and the problems of lensing survey in studying dark energy.

The article is organized as follows. In Section 2, we define the quintessence models we are considering and we recall their main properties. We also compare them to various parameterizations proposed in the literature. Section 3 focuses on cosmic shear. After a reminder on theoretical issues, we describe the weak lensing data used for our analysis and the computational pipeline, finally we outline the likelihood analysis on real (§ 3.5) and synthetic (§ 3.6) datasets. In Section 4 we combine weak lensing data with type Ia supernovae and CMB temperature anisotropies; Figure 10 and Table 1 summarize the constraints on quintessence parameters. We finish, in Section 5, by an estimation of the proficiency of two possible space-based wide field imagers to unveil the nature of dark energy.

2. Modelling dark energy

2.1. Quintessence models

In this work, we consider the simplest class of quintessence models (Ratra & Peebles 1988; Wetterich 1988) in which a scalar field Q is slow-rolling in a runaway potential. Numerous forms of potentials have been proposed but we restrict to two classes of potentials. Let us briefly summarize the properties of these models.

The first class of potentials is an inverse power law (Ratra & Peebles 1988; Wetterich 1988)

$$V(Q) = M^4(Q/M_p)^{-\alpha}, \quad (2)$$

often quoted as Ratra-Peebles (RP) potential. $M_p \equiv (8\pi G)^{-1/2}$ is the reduced Planck mass. The potential depends on two free parameters: α is a positive index while M is a mass scale that has to be adjusted to fit Ω_Q today, once α is given. In particular, if Ω_Q dominates today then M and α are related by

$$\log\left(\frac{M}{1\text{ GeV}}\right) \sim \frac{19\alpha - 47}{4(\alpha + 1)}. \quad (3)$$

The second class of potential is an extension of the previous that takes supergravity (SUGRA) corrections into account when $Q \sim M_p$ (Brax & Martin 1999),

$$V(Q) = M^4(Q/M_p)^{-\alpha} \exp(Q^2/2M_p^2). \quad (4)$$

Both potentials have a similar dynamics as long as $Q \ll M_p$ but differs at low redshift, in particular concerning their equation of state. In the SUGRA case, it is pushed toward -1 and one expects $w_0 \sim -0.82$ (Brax & Martin 1999).

With such well-defined models, the dynamics of the background is completely characterized by the Klein-Gordon equation for the scalar field,

$$\ddot{Q} + 3H\dot{Q} + \frac{dV}{dQ} = 0, \quad (5)$$

in addition to the Friedmann equation

$$\left(H^2 + \frac{K}{a^2}\right) = \frac{8\pi G}{3} \left[\rho_m + \rho_r + \frac{\dot{Q}^2}{2} + V(Q)\right] \quad (6)$$

allowing for this new matter contribution. These equations characterize background and low redshift observations and in particular the linear growth factor. Let us stress that, at this level of description, one can describe the quintessence component as a fluid with a time-dependent equation of state. This is due to the fact that the speed of sound, c_s^2 , is given by

$$c_s^2 = 1 + \frac{4}{3} \frac{1}{H\dot{Q}} \frac{dV}{dQ} \quad (7)$$

and that the equation of state evolves as

$$\dot{w} = -3H(1+w)(c_s^2 - w). \quad (8)$$

These models share the interesting property to possess scaling solutions which are attractor of the dynamical evolution. In general, but depending on the initial conditions, the dynamics starts with an early kinetic phase ($\dot{Q}^2 \gg V$) in which $w \sim 1$ so that $\rho_Q \propto (1+z)^6$. The field behaves as $Q = Q_i - A(1+z)$ and it freezes to a constant value. Since the kinetic energy decreases while the potential remains constant, this regime cannot last

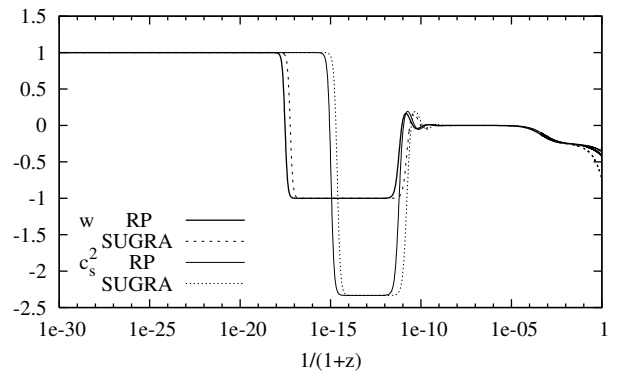


Fig. 1. Evolution of the equation of state w and of the sound speed c_s with the redshift for an inverse power law quintessence model with $\alpha = 6$, including or not the supergravity correction. We recover, from high to low redshift, the kinetic, slow-rolling and tracking phases described in the text.

forever. When the potential starts dominating, the equation of state shifts suddenly to $w \sim -1$. During this transition regime, $\rho_Q \propto (1+z)^0$. Then, there is a potential regime that lasts until the tracking regime during which

$$w = c_s^2 = \frac{\alpha w_B - 2}{\alpha + 2} \quad (9)$$

where w_B stands for the equation of state of the fluid dominating the background. At that stage, the scalar field is slow-rolling so that $w < 0$. Fig. 1 depicts the evolution of w and c_s^2 during these various regimes.

When cosmic microwave background anisotropies and large scale structures are considered, one needs to include the description of the evolution of the perturbations, and in particular include those of the scalar field described by

$$\delta\ddot{Q} + 3H\delta\dot{Q} + \left(\frac{k^2}{a^2} + \frac{d^2V}{dQ^2}\right)\delta Q + S = 0 \quad (10)$$

where S encodes the perturbations of the metric of the space-time and k is the comoving wavenumber of the perturbation. It was shown (Brax et al. 2000; Riazuelo & Uzan 2002) that there exists an attraction mechanism for super-Hubble wavelength so that the spectrum is insensitive to the initial conditions for the scalar field.

2.2. Models and parameterizations

Most data, and in particular supernovae data, are being analyzed using a general parameterization of the equation of state. These parameterizations are useful to extract model-independent information from the observations but the interpretation of these parameters is not always straightforward. In this paragraph, we remind the properties of some interesting parameterizations and compare them to the quintessence models we are considering.

Let us first recall that general parameterizations of the equation of state as

$$w(a) = w(a_0) + [w(a_m) - w(a_0)] \Gamma(a, a_t, \Delta) \quad (11)$$

were shown to allow an adequate treatment of a large class of quintessence models (Corasaniti & Copeland 2003; Basset et al. 2002). Such a parameterization involves four parameters $\{w(a_0), w(a_m), a_t, \Delta\}$ and a free function Γ varying smoothly between one at high redshift to zero today. Even though it reproduces the equation of state of most quintessence models, it is not economical in terms of number of parameters since most quintessence potentials involve one or two free parameters. If one assumes that the parameterization is supposed to describe the dynamics of a minimally coupled scalar field, the knowledge of w is sufficient but in a more general case one would need more information: The background dynamics depends on the potential and its first derivative, which can be related to w and \dot{w} . Accounting for perturbations, one needs to know the second derivative of the potential [see Eq. (10)] which can be inferred from \ddot{w} (Dave et al. 2002).

Since we expect dark energy to have observable consequences on the dynamics only at late time, one can consider

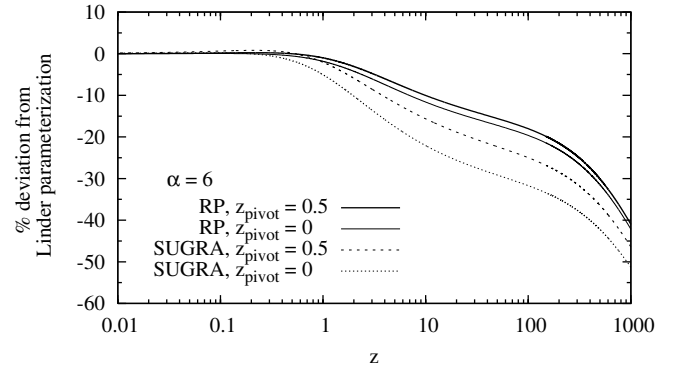


Fig. 2. Deviation of quintessence equation of state for Ratra-Peebles (solid) and SUGRA (dotted) models with $\alpha = 6$ from the generalized parameterization, Eq. (11), setting $z_{\text{pivot}} = 0$ (thick) or $z_{\text{pivot}} = 0.5$ (thin). Fitting the previous one up to $z \lesssim 0.3$, a deviation larger than 2% occurs at $z \approx 1$ for Ratra-Peebles models while at $z \approx 0.5$ for SUGRA models.

an equation of state obtained as a Taylor expansion around a pivot point,

$$w(a) = w_{\text{pivot}} + w_a(a_{\text{pivot}} - a). \quad (12)$$

This form depends on only two parameters and is a generalization of the parameterization proposed by Chevallier & Polarski (2001) and then Linder (2003) where $a_{\text{pivot}} = 1$. Two considerations are in order when using such a parameterization. First, the redshift band on which this is a good approximation of the equation of state is unknown. Clearly, compared with the form (11), it is unlikely to describe dark energy up to recombination time; see Fig. 2. Secondly, when combining observables at different redshift such as weak lensing, Sn Ia and CMB, one should choose the value of a_{pivot} in such a way that the errors in w_{pivot} and w_a are uncorrelated (Hu & Jain 2004). It follows that the pivot redshift is the redshift at which w is best constrained. In particular it was argued that it is important to choose $a_{\text{pivot}} \neq 1$ for distance-based measurements. The problem lies in the fact that the pivot redshift is specific to the observable. In this respect, dark energy models defined by a Lagrangian are more suitable, yielding to a definite equation of state as a function of redshift, hence more general than a Taylor expansion around a pivot point. Eventually, one can read out the values of w_{pivot} and w_a at whatever redshift. Fig. 3 depicts the value of w_{pivot} and w_a for the quintessence models we use, Eqs. (2) and (4), for the pivot redshifts $z_{\text{pivot}} = 0$ and $z_{\text{pivot}} = 0.5$. This complication, arising when one wants to combine datasets with different z_{pivot} , will also make it more difficult to infer constraints on the physical models from the constraints on the parameterization.

There is an alternative way to get a first hint on the nature of dark energy. It may be useful to consider the plane (w, w') where $w' \equiv dw/d \ln a$ is the derivative of w with respect to the number of e -folds. It was recently shown by Caldwell & Linder (2005) and Scherrer (2005) that quintessence models occupy a narrow part of this plane. This can be understood from Eq. (8) which implies that $w' + 3(1 - w^2) = 3(1 + w)(1 - c_s^2)$. For

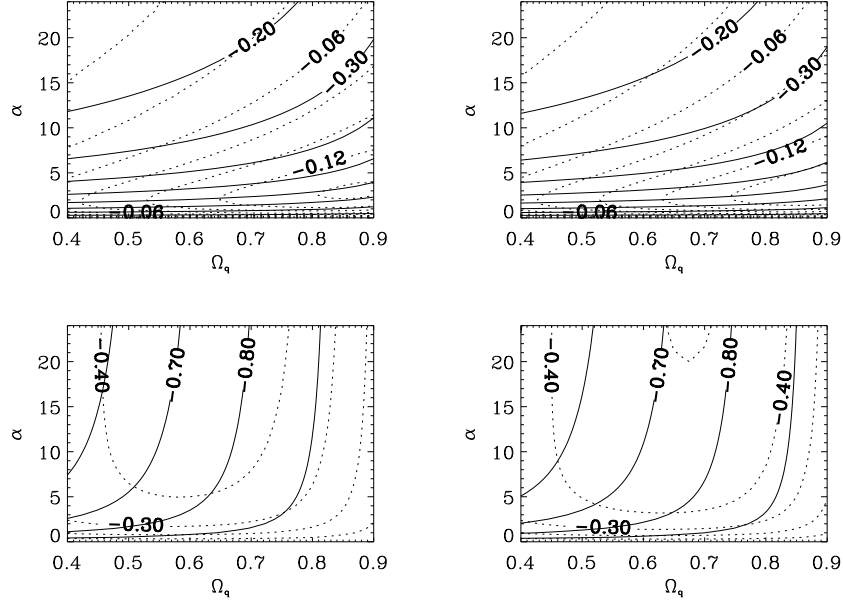


Fig. 3. Contour plots of the quintessence equation of state. We compare the equation of state of two quintessence models with the parameterization (12) for two values of the pivot redshift: $z_{\text{pivot}} = 0$ (left) and $z_{\text{pivot}} = 0.5$ (right). Solid lines correspond to level contours for w_{pivot} while dotted lines correspond to level contours of w_a . We have chosen the spacing of all the contour lines to be $\Delta w = 0.1$, except for the plots in the upper line, where $\Delta w_a = 0.02$. The upper line corresponds to Ratra-Peebles models, Eq. (2), while the lower line corresponds to SUGRA models, Eq. (4). Due to the exponential correction, w_0 is always smaller for SUGRA models because the potential is flatter and the field is rolling slower. Also, the value of w_{pivot} and w_a are more sensitive to the choice of z_{pivot} for SUGRA models than for Ratra-Peebles models.

quintessence models, $1 + w > 0$, and Eq. (7) implies that $c_s^2 < 1$ (because $\dot{Q} > 0$ and $V' < 0$) so that

$$w' > -3(1 - w^2), \quad (13)$$

without any assumptions on the dynamics of the scalar field. In Caldwell & Linder (2005), two classes of quintessence models were exhibited, namely “thawing” models, in which $w \sim -1$ initially and increases as Q rolls down the potential, and “freezing” models, in which $w > -1$ initially and tends toward -1 as Q rolls down the potential. “Freezing” models contain tracking models and in particular the Ratra-Peebles models, Eq. (2), and SUGRA models, Eq. (4), considered in this work. Using a combination of numerical simulations and physical arguments, they concluded that

$$3w(1 + w) < w' < 0.2w(1 + w) \quad (14)$$

for “freezing” models. From an observational point of view, the analysis of supernovae data (Riess et al. 2004) showed that if the universe is flat then $w_0 = -1.31^{+0.22}_{-0.28}$ and $w'_0 = -1.48^{+0.90}_{-0.81}$ after marginalizing on Ω_{m0} . If one further imposes that $w_0 > -1$ then $w_0 < -0.76$ and $w'_0 = -0.6 \pm 0.5$. In the case where w is assumed constant then $w = -1.02^{+0.13}_{-0.19}$ and $w < -0.72$ at 68% and 99% confidence level respectively.

This phase-space analysis creates a link between the various parameterizations and the physical models. It can be shown (Scherrer 2005) that different classes of models (e.g. k-essence, Chaplygin gaz, quintessence, etc.) lies in different parts, hence offering a way to distinguish between these models

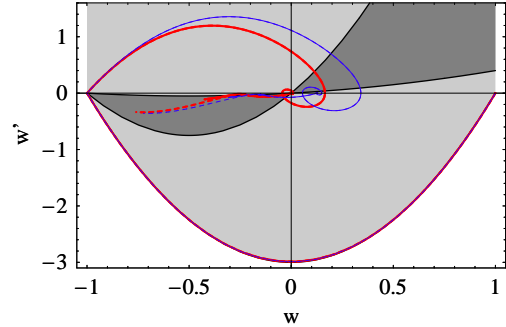


Fig. 4. Dynamics of the two quintessence models in the plane (w, w') . The shaded regions correspond to the constraints (13) in light gray and (14) in dark gray. We have considered a Ratra-Peebles (solid) and SUGRA (dash) models with $\alpha = 6$ (thick/red) and $\alpha = 11$ (thin/blue). Only in the tracking regime the models are compatible with Eq. (14).

without measuring $w(z)$. In particular, Fig. 4 depicts the dynamics of some Ratra-Peebles and SUGRA models in the (w, w') plane, superposed to the regions where the inequalities (13) and (14) hold. Notice that the trajectories for the SUGRA potential are essentially the same of the Ratra-Peebles one, deviating just at low redshift towards the cosmological constant solution.

2.3. Summary

Quintessence models require only *two* parameters to describe the whole dynamics (with no redshift limitation). Compared to a pure cosmological constant, described by only one number, this gives us one extra parameter. In terms of extra-parameter with respect to a standard Λ CDM, this is equivalent as considering a constant equation of state for dark energy.

On the other hand, a parameterization of the equation of state of the dark energy is sufficient to describe the low redshift universe. But, the parameterizations which describe accurately quintessence models involve at least *four* extra-parameters. It is thus more economical to work directly with the physical model. In that case, the evolution of perturbations can be inferred from w but this is not the case in more general situations.

Parameterizations with fewer parameters have a smaller dynamical range and are likely to be bad descriptions of dark energy at high redshift, notably for CMB computation. Besides, when combining dataset, the choice of the pivot redshift may induce some difficulties in interpreting the constraints on the parameters in terms of constraints on the physical models.

So considering directly a well-defined physical model instead of a parameterization is economical concerning the number of extra-parameter and avoids the problem of the pivot redshift. It allows us to compute the prediction of the models at all redshift (Sn Ia, weak lensing, and CMB). On the other hand, it concerns only a small class of models.

This discussion shows that both routes are complementary. In particular, it would be worth to evaluate to which accuracy constraints of order 1% on a given parameterization constrain physical models.

3. Cosmic shear

Gravitational lensing by large scale structures of the universe produce weak distortion fields and collectively modify the shape of background galaxies (see e.g. Bartelmann & Schneider 2001; Mellier 1999; Réfrégier 2003). Though this is a very weak signal and a challenging task, it has been detected almost simultaneously by van Waerbeke et al. (2001), Wittman et al. (2000), Kaiser et al. (2000), Bacon et al. (2000) and it now routinely observed by many groups around the world (see van Waerbeke & Mellier 2003; Hoekstra 2003 for recent reviews on observations). Over the past years the huge efforts carried out by these groups to deal with critical systematics considerably improved the reliability of the lensing signal and strengthened the ability of cosmic shear to constrain cosmological models from the statistical analyses of galaxy ellipticities.

3.1. Generalities

The gravitational lensing effect depends on the second order derivatives of the gravitational potential. The convergence, κ , and the shear, $\gamma = (\gamma_1, \gamma_2)$, describe the distortion of back-

ground images by the matter along the line of sight. These components are related by

$$\Delta\kappa = (\partial_1^2 - \partial_2^2)\gamma_1 + 2\partial_1\partial_2\gamma_2. \quad (15)$$

The evolution of the convergence is dictated by the Sachs equation (Sachs 1962; see Uzan & Bernardeau 2000 for a more modern description). The convergence in the direction θ can be related to the matter distribution integrated along the line of sight

$$\kappa(\theta, \chi) = \frac{3}{2} \frac{\Omega_{m0} H_0^2}{c^2} \int_0^\chi \frac{S_K(\chi - \chi') S_K(\chi')}{S_K(\chi)} \times \frac{\delta_m[S_K(\chi')\theta, \chi']}{a(\chi')} d\chi' \quad (16)$$

for sources located at a radial distance χ defined by

$$\chi(z) = \int_0^z \frac{dz'}{H(z')} \quad (17)$$

and S_K is the angular diameter distance given by

$$S_K(\chi) = \begin{cases} \sin(\sqrt{K}\chi)/\sqrt{K} & K > 0 \\ \chi & K = 0 \\ \sinh(\sqrt{-K}\chi)/\sqrt{-K} & K < 0 \end{cases}. \quad (18)$$

If the sources have a distribution given by $n_\chi(\chi)d\chi = n(z)dz$ then the effective convergence takes the form

$$\kappa(\theta) = \int_0^{\chi_H} n_\chi(\chi) \kappa(\theta, \chi) d\chi \quad (19)$$

where χ_H is the comoving radial distance of the horizon. Decomposing the convergence in 2-dimensional Fourier modes,

$$\kappa(\theta) = \int \frac{d^2\ell}{2\pi} \hat{\kappa}(\ell) e^{i\ell \cdot \theta}, \quad (20)$$

the shear power spectrum, defined by $\langle \hat{\kappa}(\ell) \hat{\kappa}(\ell') \rangle = P_\kappa(\ell) \delta^{(2)}(\ell + \ell')$, can be related to the 3-dimensional power spectrum of matter density perturbations P_m by

$$P_\kappa(\ell) = \frac{9}{4} \frac{H_0^4 \Omega_{m0}^2}{c^4} \int_0^{\chi_H} \left[\frac{g(\chi)}{a(\chi)} \right]^2 P_m \left[\frac{S_K(\chi)}{\ell}, \chi \right] d\chi \quad (21)$$

in the small angle approximation (see e.g. Bartelmann & Schneider 2001, Peter & Uzan 2005 chap. 7). The function g is given by

$$g(\chi) = \int_\chi^{\chi_H} n_\chi(\chi') \frac{S_K(\chi' - \chi)}{S_K(\chi')} d\chi'. \quad (22)$$

Note that the window function $W(z) \equiv [g(\chi)/a(\chi)]^2$ is peaked around $z \simeq z^*/2$ for a distribution of sources $n(z)$ approximately peaked at redshift z^* . This will be useful in the choice of the pivot redshift. Let us stress that expressions (16) and (21) assume the validity of the Poisson equation and thus of general relativity. These expressions may be slightly different in more general contexts and even be used to test general relativity (see Uzan & Bernardeau 2001; Schmid et al. 2005).

Neither κ nor P_κ are directly observable, but only filtered quantities can be obtained. Cosmic shear can be measured by

various types of 2-point statistics which differ only by the chosen filtering scheme. This implies that their sensitivity to the power spectrum, and also to systematics, are different. In this work we consider two of these statistics, namely the aperture map variance, defined by

$$\langle M_{\text{ap}}^2 \rangle(\theta_c) = \frac{288}{\pi} \int \ell P_{\kappa}(\ell) \left[\frac{J_4(\ell\theta_c)}{\ell^2\theta_c^2} \right]^2 d\ell, \quad (23)$$

which is a bandpass estimate of the convergence power spectrum, and the top-hat shear variance

$$\langle \gamma^2 \rangle(\theta_c) = \frac{8}{\pi} \int \ell P_{\kappa}(\ell) \left[\frac{J_1(\ell\theta_c)}{\ell\theta_c} \right]^2 d\ell, \quad (24)$$

which is a lowpass estimate of P_{κ} . Here J_n are the Bessel functions of the first kind. Both statistics can be deduced from two linear combinations of the radial and tangential components of the shear variance, $\xi_{\pm} \equiv \langle \gamma_{\text{t}}^2 \rangle \pm \langle \gamma_{\text{r}}^2 \rangle$ (see e.g. Bartelmann & Schneider 2001), which are directly estimated from the shapes of background galaxies.

3.2. Matter power spectrum and non-linear regime

In the previous expressions, and in particular in Eqs. (16) and (21), P_{m} refers to the full 3-dimensional power spectrum of pressureless matter, including cold dark matter and baryons.

In the linear regime, the growth factor D_+ is the growing solution of

$$\ddot{D}_+ + 2H\dot{D}_+ - \frac{3}{2}H^2\Omega_{\text{m}}D_+ = 0. \quad (25)$$

The second term that describes the damping due to the cosmological expansion contains all the effect of dark energy on D_+ . In this regime, the total effect on lensing, Eq. (21), is similar to the one obtained from a single redshift plane (see Benabed & van Waerbeke 2003; Schmid et al. 2005) so that the integrated growth effect is degenerated with the normalization of the spectrum.

Dealing with low-redshift sources, the lensing predictions and analysis involve the non-linear power spectrum. This regime cannot be described analytically from a perturbation approach (see however the proposal by Crocce & Scoccimarro 2005) and one would need to rely on N -body simulations.

N -body simulations including quintessence were recently performed using the GADGET code (Dolag et al. 2003) or an adaptive refinement tree code (Klypin et al. 2003). It was argued by Dolag et al. (2003) that the halo concentration distribution around the mean value does not depend on the cosmology, while the concentration parameter depends on the dark energy equation of state at the cluster formation redshift through the linear growth factor. However a systematic study confirming this claim is lacking. Klipin et al. (2003) and Mainini et al. (2003) show that dark energy changes the virial density contrast, Δ_c , which induces a change in the power spectrum at small scales ($k \gtrsim 1h\text{Mpc}^{-1}$) but, for constant w , the error is smaller than the error in the expected non-linear model (Jarvis et al. 2005).

Instead of specific N -body simulations accomodating quintessence, in order to compute the non-linear matter power spectrum one can deal with linear-to-non-linear mappings, for instance based on the stable clustering *ansatz* (Hamilton et al. 1991; Peacock & Dodds 1996) or to a halo model (e.g. Ma & Fry 2000; Seljak 2000; Smith et al. 2003). These mappings have been tested for several cosmologies including ΛCDM but not for dynamical dark energy models. Given their robustness and the precision level we can actually reach, we can hope that they remain valid for the class of models we are considering. Indeed this is a very strong assumption that can be justified by the fact that we do not expect the scalar field to cluster on small scales so that it is unlikely to affect the small scale behaviour of matter but by its influence on the expansion rate. Arguing that the clustering scale of the quintessence field is given by its Compton wavelength, Ma et al. (1999) propose an analytic approximation for the Peacock & Dodds (1996) formula to include quintessence with constant equation of state, claiming a 10% level accuracy. McDonald et al. (2005) propose a recipe to extend the aforementioned mappings to $w \neq -1$ cases, attaining a better accuracy for $k \lesssim 10\text{Mpc}^{-1}$ by systematically exploring a wider parameter space. Nevertheless, upcoming weak lensing measurements require an improved description of the smaller scales physics (Huterer & Takada 2005), eventually including hydrodynamics (Zhan & Knox 2004; Jing et al. 2005).

In conclusion, it seems early to decide how dark energy, and quintessence in particular, modify the mapping calibrated on ΛCDM . For that reason, in this work we will consider two linear-to-non-linear mappings, by Peacock & Dodds (1996) and Smith et al. (2003), and try to identify the parameters that are not sensitive to this choice. We will also try to quantify how the other parameters are affected so that we can estimate how our ignorance of the non-linear regime limits the use of weak lensing.

Hopefully, as we will also show, weak lensing data in the linear regime shall be able to be used. In that case, we can get an interesting constraint on the growth factor without messing with non-linear physics.

3.3. Lensing data

We use three sets of data for weak lensing, the VIRMOS-Descart (van Waerbeke et al. 2005), the deep field of the CFHTLS survey (Semboloni et al. 2005) and the wide field of CFHTLS (Hoekstra et al. 2005).

The details regarding the survey properties, image and catalogue processing of VIRMOS-Descart data are described in van Waerbeke et al. 2001 and McCracken et al. 2003. The shear measurement and error analysis are described in van Waerbeke et al. 2005 and summarized in Table 2 of that paper. This survey covers an effective (the unmasked area) area of 8.5deg^2 spread in four fields. It probes lensed galaxies down to the limiting magnitude $I_{AB} = 24.5$ has an effective galaxy number density (after all selection processes) of 15gal/arcmin^2 , and explores angular scales up to 50 arc-minutes.

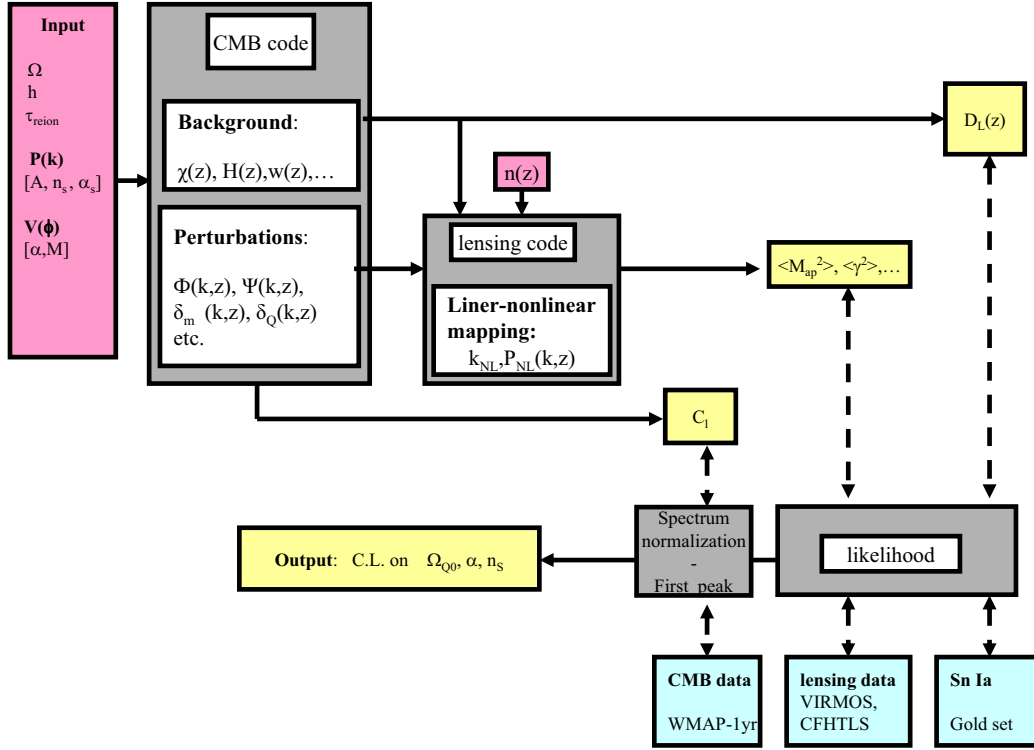


Fig. 5. Pipeline implemented for this work. Presently, we restrict to three free cosmological parameters, $\{\Omega_{Q0}, \alpha, n_s\}$, keeping fixed the others. The lensing code manipulates both background's and perturbations quantities computed by the CMB code, using a sources distribution $n(z)$ depending on the used dataset. In particular, the source redshift parameter z_s is left to vary and marginalized over afterwards. Finally, the likelihood is computed using (either real or synthetic) cosmic shear and Sn Ia data, both separately and jointly. The temperature CMB data are used to fix the amplitude A of the power spectrum at decoupling, and to put (conservative) constraints on the (Ω_{Q0}, α) parameters sub-space using the location of the first peak. In the CMB section of the pipeline, we indicate by δ_m and δ_Q energy density fluctuations in matter and quintessence components, respectively, while $\Phi(k, z)$ and $\Psi(k, z)$ are the scalar perturbations of the metric (Bardeen potentials) in Fourier space. In the lensing section, we denote by k_{NL} the scale at which the power spectrum becomes non-linear, $P(k_{NL}, z) \sim 1$. See § 3 for details.

For the CFHTLS deep and wide, all relevant details are given in Semboloni et al. 2005 and Hoekstra et al. 2005, respectively. The deep covers an effective area of 2.2 deg^2 in three fields, down to $I_{AB} = 26$, but only samples angular scales up to 30 arc-minutes. The effective galaxy number density is 22 gal/arcmin^2 . In contrast, the wide has a much larger effective area than the deep (22 deg^2) but only spread in two fields. It explores angular scales up to one degree at about the same depth as VIRMOS-Descart. The effective galaxy number density is 13 gal/arcmin^2 (the final selection produced a catalogue somewhat less deep than VIRMOS-Descart). Note that once completed the wide survey will be composed of three compact areas that will sample angular scales up to 5 degrees in three independent fields so that linear scales will be explored with much more accuracy than present-day CFHTLS wide data.

Each survey used complementary photometric or spectroscopic galaxy samples to derive the redshift distribution of the lensed galaxy samples. As discussed in the VIRMOS-Descart

and CFHTLS cosmic shear papers, it is convenient to describe the redshift distribution by a three-parameter function

$$n(z) = \frac{\beta}{z_s \Gamma\left(\frac{1+\alpha}{\beta}\right)} \left(\frac{z}{z_s}\right)^\alpha \exp\left[-\left(\frac{z}{z_s}\right)^\beta\right]. \quad (26)$$

α and β are obtained from a fit of photometric redshift distributions derived from external redshift calibration surveys. The CFHTLS and VIRMOS are different lensing data sets, but they were obtained with the same telescope (although with different instruments) and with the same exposure time. Therefore the two lensing surveys have to be calibrated using the same external redshift data set in order to preserve the homogeneity of the analysis. In van Waerbeke et al. (2005), VIRMOS was calibrated using the Hubble Deep Fields and MS1008 (see van Waerbeke et al. 2001 for the details), while the CFHTLS lensing data (Hoekstra et al. 2006; Semboloni et al. 2006) were calibrated using the HDF only. The HDF and MS1008 data in visible and near infrared bands produced accurate photometric redshifts (Yahata et al. 2000; Athreya et al. 2002). We decided to use the HDF only for both VIRMOS and CFHTLS and abandon the MS1008 field. We have checked that the re-

sults discussed in this paper do not depend whether or not we include the MS1008 calibration field, since the sample variance due to the use of combined redshift calibration sets is absorbed in the redshift error (van Waerbeke et al. 2006).

In the following, we will use for the CFHTLS-deep survey (Semboloni et al. 2005)

$$\alpha = 1.9833, \quad \beta = 0.6651, \quad z_s = 0.0981^{+0.0129+0.0209}_{-0.0114-0.0161} \quad (27)$$

giving a mean redshift $\langle z \rangle = 1.01$, while for the CFHTLS-wide and the VIRMOS-Descart surveys (Hoekstra et al. 2005)

$$\alpha = 1.35, \quad \beta = 1.654, \quad z_s = 0.668^{+0.035+0.053}_{-0.036-0.055} \quad (28)$$

giving a mean redshift $\langle z \rangle = 0.76$. We quote the 1σ and 2σ errors. We use the same parameters for the VIRMOS-Descart and CFHTLS-wide redshift distributions since both surveys have a similar depth and the same effective galaxy number density.

3.4. Description of the pipeline and choice of the free parameters

The pipeline we developed is summarized in Fig. 5. We compute the evolution of background and perturbations power spectra in linear regime by means of a Boltzmann code allowing for photons, neutrinos, baryons, cold dark matter and quintessence scalar field. Notice that this code deals with several gauge choices and can also account for scalar-tensor theories of gravity (Riazuelo & Uzan 2002), hence allowing to study deviations from general relativity in this framework as well as extended quintessence scenarios (Uzan 1999; Amendola 2000; Chiba 1999).

Using this code we compute the CMB temperature (TT) angular power spectrum (C_ℓ) in order to fix the amplitude of the initial matter power spectrum at the redshift of the last scattering. We do it by matching the computed C_ℓ with WMAP-1yr data (Hinshaw et al. 2003) at a high multipole, to be preferred when studying quintessence since at low multipoles the integrated Sachs-Wolfe effect is dominant so that temperature anisotropies are not directly related to the density perturbations. Definitely, we use the multipole $\ell \simeq 110$ of WMAP-1yr data, where the total relative error of the TT spectrum is smaller than 3%. This normalization procedure holds until the correlation between multipoles is weak and does not take into account the measurement errors on the amplitude of the TT spectrum. However, we expect that the final results would not be strongly affected by a more accurate normalization. Notice that, as mentioned earlier on, σ_8 data is not used to normalize the spectrum. Hence, its value may be evaluated from the matter power spectrum and compared with the observed values.

Once the linear matter power spectrum is known at every redshift, the weak lensing add-on code (Schimd et al. 2005) computes the non-linear power spectrum using two mappings, by Peacock & Dodds (1996) and Smith et al. (2003). We consider wavevectors ranging up to $10 h \text{ Mpc}^{-1}$ (corresponding to 1 arcmin at $z \sim 1$ for cosmologies close to ΛCDM). By Limber projection, we deduce the shear power spectrum allowing for a source redshift distribution of the form (26). To finish, several two-point statistics in real space are computed, namely the top-hat shear variance $\langle \gamma^2 \rangle$, the aperture mass variance $\langle M_{\text{ap}}^2 \rangle$, as

well as the two-point correlations ξ_{\pm} . Let us stress that, like the Boltzmann code, the lensing add-on code works with scalar-tensor theories of gravity as well.

Cosmological parameters are estimated by comparing the predicted signal m_i to the data d_i as a function of scale X_i (which reduces to an angular scale θ_i , a redshift z_i or a multipole ℓ_i respectively for lensing, supernovae and CMB data). We vary the parameters of the model, disposing them on a regularly spaced grid and evaluate, at each grid point, the likelihood function,

$$\mathcal{L} = \frac{1}{(2\pi)^n |C|^{1/2}} \exp \left[-\frac{1}{2} (d_i - m_i)^T C^{-1} (d_i - m_i) \right]. \quad (29)$$

Here C^{-1} is the data covariance matrix, including Poisson shot noise and cosmic variance.

We focus on constraining the dark energy density and the parameter α of the quintessence potentials and restrict to a low-dimensional parameter space. Ideally, one would include at least nine cosmological parameters: the spatial curvature, the Hubble constant, the parameter α of the potential, the dark energy and matter (both dark matter and baryonic) density parameters, the reionization optical depth, the amplitude and spectral index of the initial power spectrum. In addition, one should include the three parameters accounting for the redshift distribution of sources, Eq. (26).

Given the result of the analysis of CMB data (Spergel et al. 2003) we have assumed a spatially flat universe so that $\Omega_{\text{m}0} = 1 - \Omega_{\text{Q}0}$. The amplitude of the initial power spectrum is fixed by the normalization on the CMB. We have also assumed that the reduced Hubble constant, the reionization optical depth, and the baryon energy density today are fixed to $h = 0.72$, $\tau_{\text{reion}} = 0.17$, and $\Omega_{\text{b}0} h^2 = 0.024$, respectively.

We preliminarily performed a Fisher matrix analysis on the parameters space $(\alpha, \Omega_{\text{Q}0}, n_s)$ in order to estimate approximately the extent of the 1σ region and decide the sampling steps of the grid for the computation of the likelihood. Figure 6 depicts the 68%, 95%, and 99% confidence levels (C.L.) after for cosmic shear (top-hat variance) corresponding to a synthetic CFHTLS-wide like survey covering 170 deg^2 , with $20 \text{ galaxies/arcmin}^2$ and an intrinsic ellipticity of 0.4. The top line refers to Ratra-Peebles models and the bottom line to SUGRA models. Interestingly, SUGRA models appear to be more constrained. Notice that the Fisher analysis holds only locally, around a fiducial model (marked by a cross) which is fixed at $\alpha = 6$, $\Omega_{\text{Q}0} = 0.73$, and $n_s = 1.0$.

In the final likelihood analysis we allow to vary the cosmological parameters in the following ranges

$$\Omega_{\text{Q}0} \in [0.4, 0.9], \quad \alpha \in [0, 25], \quad n_s \in [0.9, 1.1]. \quad (30)$$

For the cosmic shear data, we also allow one of the source redshift parameters to vary. We choose z_s , always marginalized in the final analysis, over its 2σ interval; see Eq. (27) and (28).

Indeed, one can criticize these assumptions but these are sufficient *i)* to give us an idea of the parameter space available for dark energy realized by quintessence and *ii)* to discuss to which extent weak lensing can improve the constraints on

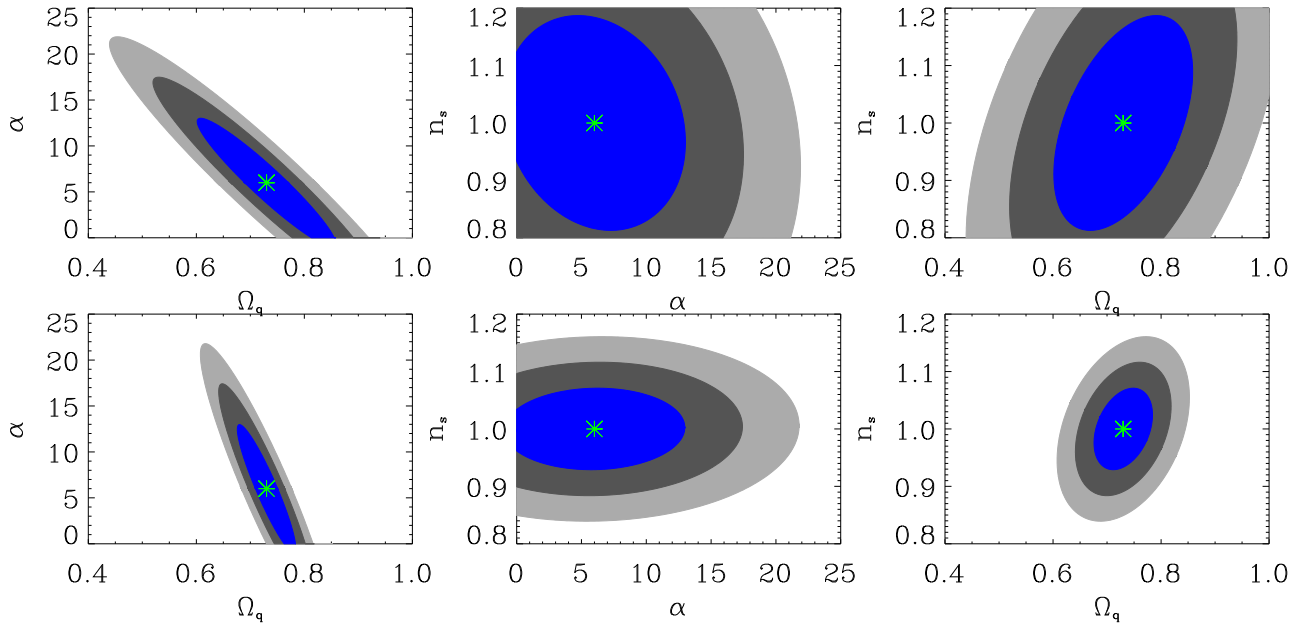


Fig. 6. Fisher analysis of the top-hat shear variance of the cosmic shear on cosmological parameters $(\alpha, \Omega_{Q0}, n_s)$, for Ratra-Peebles (top line) and SUGRA (bottom line) models – contours at 68 and 95% C.L. We employ a synthetic realization of a CFHTLS-wide like survey, covering 170 deg^2 , with 20 gal/arcmin^2 and intrinsic ellipticity $\sigma_e = 0.4$. The fiducial model is defined by $(\alpha, \Omega_{Q0}, n_s) = (6, 0.73, 1)$ while $(h, \tau_{\text{reion}}, \Omega_{b0}h^2) = (0.72, 0.17, 0.024)$ are kept fixed. The goal of this analysis is to help in choosing the range of the grid for the likelihood analysis. See § 3.4 for discussion.

dark energy models. From a pragmatic point of view, we were limited by computational capacities and a more complete analysis will follow. Let us stress that such an analysis requires an investigation of the potential degeneracies of the dark energy parameters with the standard cosmological parameters and in particular, one would need to quantify how allowing for dark energy changes the allowed range of variation of the other cosmological parameters. This is left for further studies.

3.5. Likelihood analysis: Joint cosmic shear data

Using both real and synthetic cosmic shear data, we perform the likelihood analysis aiming to investigate to which extent the constraints on cosmological parameters, and in particular the quintessence ones, depend on the linear-to-non-linear mapping and on the selection effects of the two-points statistics.

In this section, we focus on the first issue by combining top-hat variance data of VIRMOS-Desart, CFHTLS-deep and CFHTLS-wide (22 deg^2 sub-sample) surveys; see Table 1 for numerical results of individual parameters constraints. Figure 7 depicts the results quoting the 68%, 95% and 99% confidence level contours. In particular, we compute the non-linear spectra by both the Peacock & Dodds (1996) and Smith et al. (2003) procedures, for Ratra-Peebles and SUGRA models as well, hence allowing for two kinds of comparisons.

Firstly, we can compare Ratra-Peebles and SUGRA likelihood contours, disregarding the non-linear mappings. There are two striking differences. One is the strong constraint on Ω_{Q0} found in the SUGRA case. The reason for this is that, since the amplitude of the power spectrum is kept fixed, the

(σ_8, Ω_{m0}) degeneracy implies a strong constraint on Ω_{m0} and consequently on Ω_{Q0} through the flat universe prior. This effect is stronger in SUGRA models than in Ratra-Peebles ones since the former approach a Λ CDM at low redshift. The other difference is the well defined degeneracy found in the (Ω_{Q0}, α) plane for the Ratra-Peebles case. This feature will allow to put a stronger constraint on Ratra-Peebles' α than in SUGRA's α when combining with other data.

Secondly and perhaps more interestingly, by comparing the non-linear mappings, for both Ratra-Peebles and SUGRA models two classes of cosmological parameters come out: Those concerning the quintessence, α and Ω_{Q0} , are found to be essentially independent of the non-linear mapping used. This supports the claim of Simpson & Bridle (2005) that cosmic shear is sensitive to dark energy mostly through the background dynamics. The second class involves the cosmological parameters accounting for the primordial universe, here n_s only. In this case the corresponding likelihood contours strongly depend on the chosen mapping, regardless of the quintessence potential we used. Hence it seems not possible to constrain the primordial spectral index, at least jointly with quintessence parameters, until a stable formulation of the non-linear regime of structure formation will be available.

3.6. Likelihood analysis: Synthetic data

Using wide surveys, we can eventually investigate the effect of the non-linear regime of structures formation. For this purpose, we perform a likelihood analysis using a synthetic realization of the full CFHTLS-wide survey. This consists on syn-

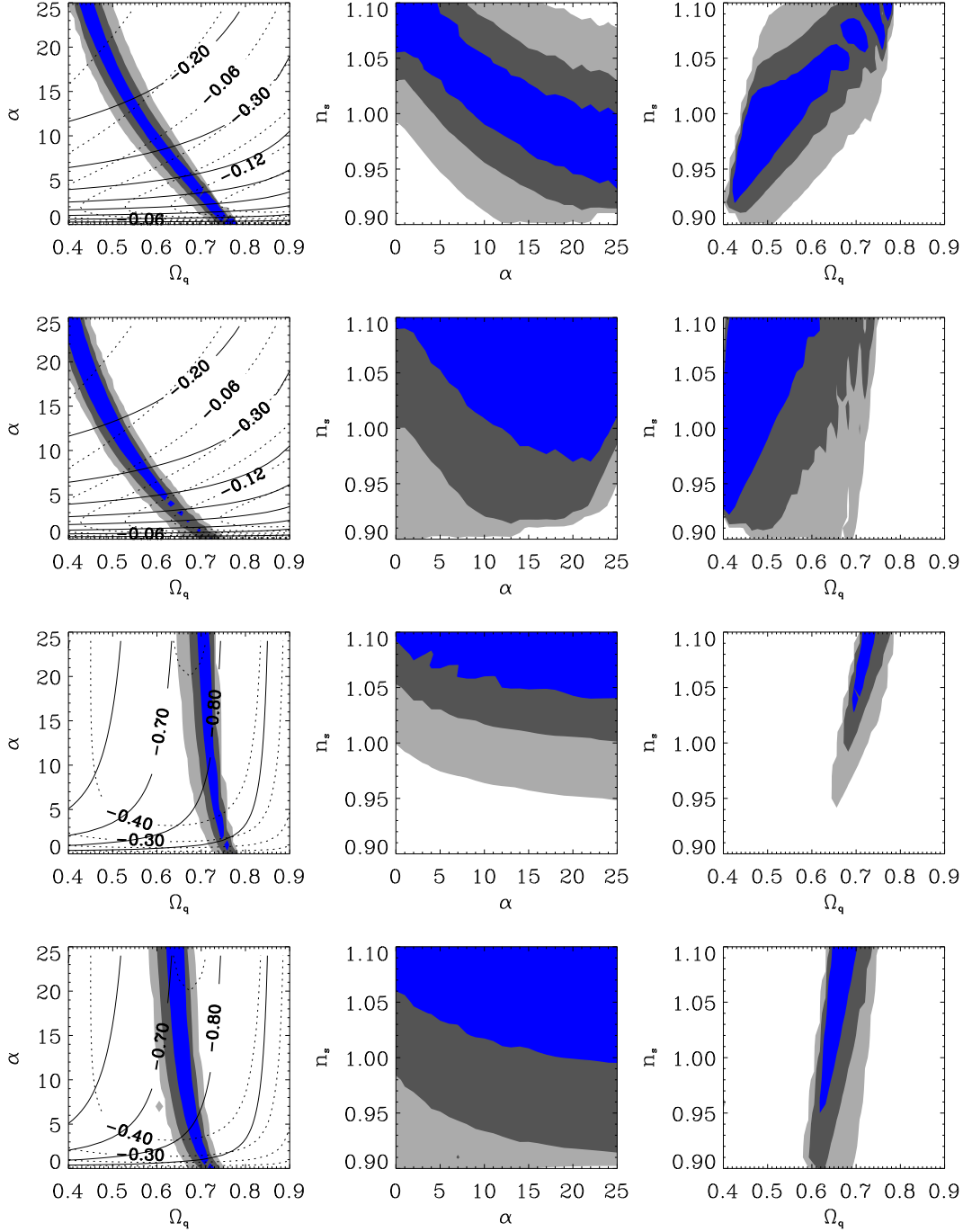


Fig. 7. Joint likelihood analysis of VIRMOS-Descart, CFHTLS-deep, and CFHTLS-wide/22 deg² top-hat variance data – contours at 68%, 95%, and 99% C.L. for the variables (Ω_{Q0}, α) , (α, n_s) and (Ω_{Q0}, n_s) . On the quintessence parameters sub-space, we have added the contour lines of (w_{pivot}, w_d) discussed in Fig. 3, assuming $z_{\text{pivot}} = 0.5$. The two upper lines are dedicated to Ratra-Peebles models [Eq. (2)] and the two lower to SUGRA models [Eq. (4)]. For each class of models, the non-linear spectrum has been computed using both the Peacock & Dodds (1996) procedure, first and third lines, and the halo model approach by Smith et al. (2003), second and fourth lines. See § 3.5 for discussion.

thetic data vectors of top-hat and aperture mass variance and on a synthetic covariance matrix. The former are computed at a fiducial model, which we take to be a Λ CDM with the current CFHTLS-wide redshift distribution. The covariance ma-

trix is computed using the analytical approximation derived in Schneider et al. (2002). It depends on three main features of the survey; the effective area A , the effective galaxy number density n_{gal} and the dispersion of the distribution of elliptici-

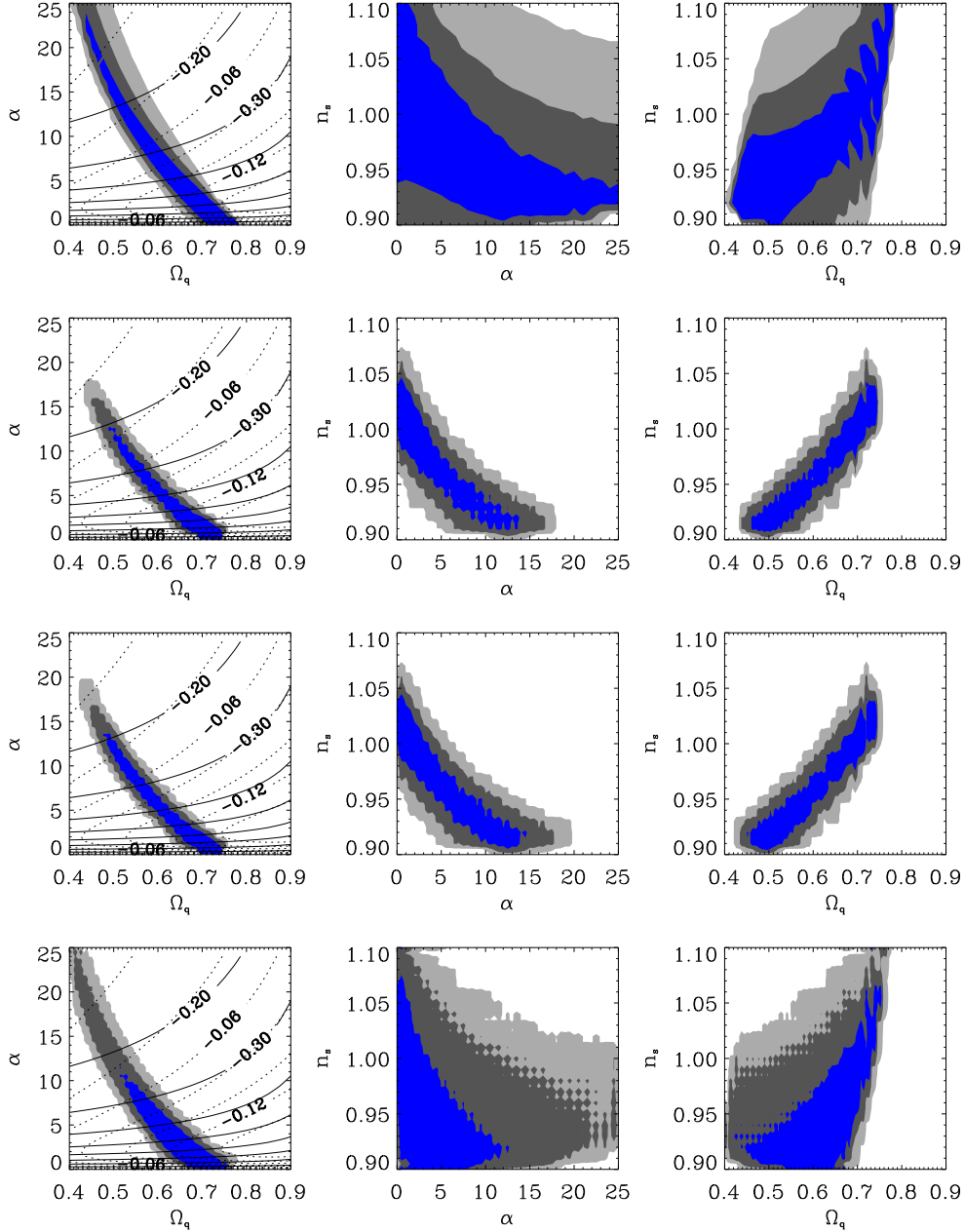


Fig. 8. CFHTLS-wide constraints on Ratra-Peebles models. From left to right, we present the likelihood analysis (68, 95, and 99% C.L.) for the variables (Ω_{Q0}, α) , (Ω_{Q0}, n_s) and (Ω_{Q0}, α) and we have added the contour lines discussed in Fig. 3, assuming $z_{\text{pivot}} = 0.5$. The first line depicts the analysis of the actual dataset based on 22 deg² (W1+W3; see § 3.6) while the three other lines are based on the synthetic data for a field of 170 deg². The second and third line show the top-hat shear variance and aperture mass variance, respectively. The fourth line describes the analysis of the same simulated data for the top-hat shear variance but using only angular scales larger than 20 arcmin to cut out the non-linear part of the matter power spectrum. In particular, we conclude from the left column that the parameters describing the quintessence sector (α and Ω_{Q0}) are not affected by the choice of the statistics and are well estimated by the linear part of the power spectrum. Here we use the Peacock & Dodds (1996) mapping for the non-linear power spectrum. See § 3.6 for discussion.

ties σ_e . For these parameters we used the values that are expected at the end of the CFHTLS-wide campaign, respectively: $A = 170 \text{ deg}^2$, $n_{\text{gal}} = 20 \text{ gal/arcmin}^2$, and $\sigma_e = 0.4$. Notice we assume a larger ellipticity dispersion and a higher density of galaxies than those obtained in Hoekstra et al. (2005). They

correspond to a different galaxy weighting scheme than the one used with current data.

Figures 8 and 9 outline the likelihood analysis of Ratra-Peebles and SUGRA models, respectively – contours at 68%, 95% and 99% confidence level. We show only the results achieved using the mapping by Peacock & Dodds (1996), those

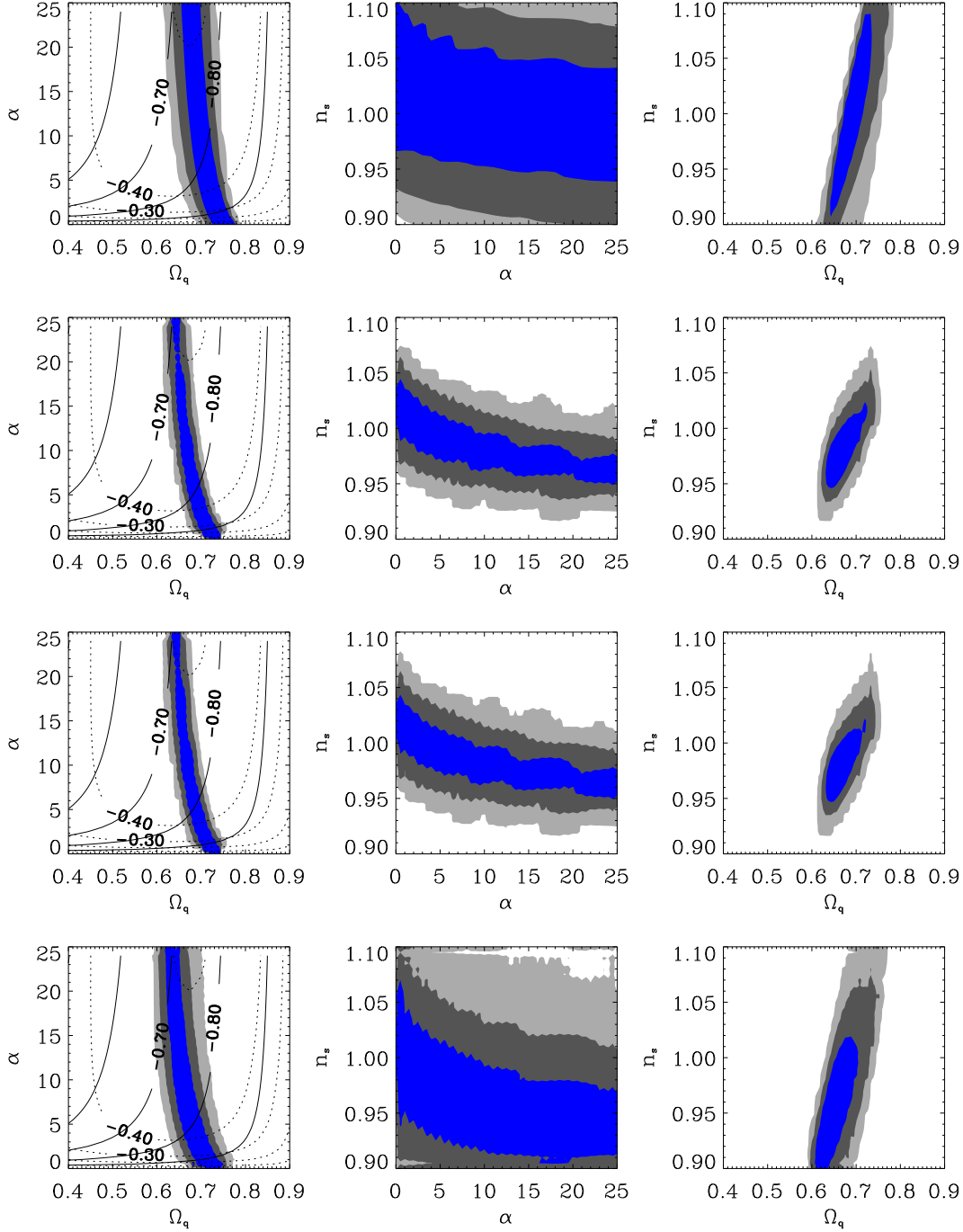


Fig. 9. CFHTLS-wide constraints on SUGRA models. This figure is analogous to Fig. 8. We reach the same conclusion as for Fig. 8. We recover that the contours are almost independent on the value of α . See § 3.6 for discussion.

achieved using the mapping by Smith et al. (2003) being in agreement at a 10% level.

Firstly, by comparing the results achieved using the top-hat variance data of the 22 deg² sub-sample (first line) with those of the synthetic 170 deg² field (second line), it is evident the gain achievable by the full survey. In particular, it is worth noticing that the pure quintessence parameters sub-space is less dependent on the survey area, while the constraints on the primordial spectral index strongly depend on it. Hence, the distinction of

cosmological parameters in two classes introduced in the previous section seems confirmed.

The second and third lines show the likelihood contours for the top-hat and aperture mass variances, respectively. They are consistent, depicting compatible confidence level regions, for both Ratra-Peebles and SUGRA models. There are two main differences in the properties of aperture mass and top-hat variances. Measurements of aperture mass variance at different scales are less correlated than top-hat variance ones, since the former is a narrow filtered version of the shear power spec-

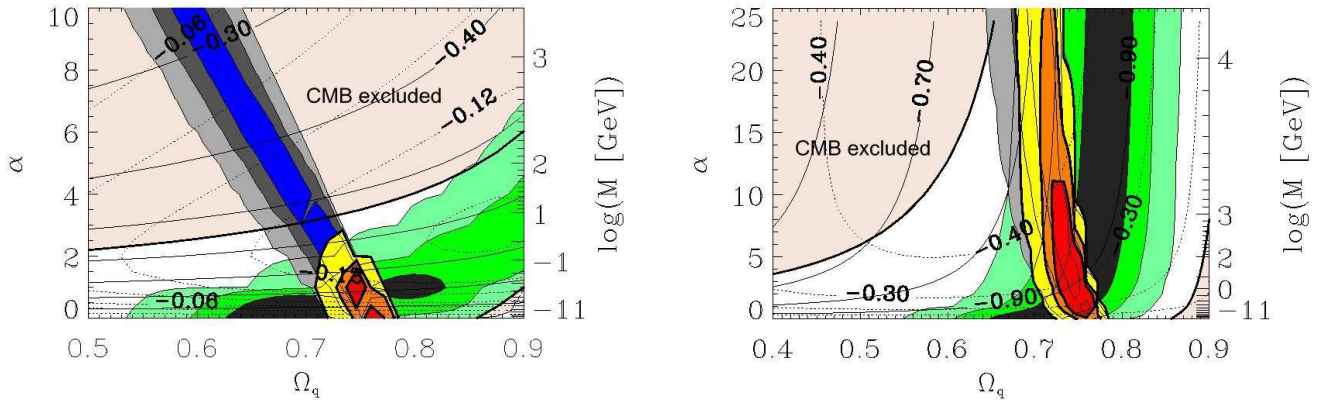


Fig. 10. Joint analysis of the quintessence parameters (Ω_{Q0} , α ,) from CMB, Sn Ia and cosmic shear (top-hat variance), for Ratra-Peebles models (left panel) and SUGRA models (right panel). The likelihood analysis uses the “gold” set for Sn Ia (green contours), VIRMOS-Descart + CFHTLS-deep + CFHTLS-wide (22 deg²) top-hat variance data for the cosmic shear (blue contours), and both combined (red contours). Contours correspond to 68, 95, and 99% C.L. According to WMAP-1yr measurements, the location of the first acoustic peak of the TT power spectrum of CMB, allowing for binning between neighboring multipoles, excludes regions of the parameter space (shadowed) nearly degenerate with Sn Ia constraints; see § 4.2 for details. On the right axes, we quote an indicative mass scale of the quintessence potential, weakly dependent on Ω_{Q0} but Ω_{Q0} is small; see § 2 for details. Finally, contours of w_{pivot} (solid) and w_a (dotted) are superposed, setting $z_{\text{pivot}} = 0$. As for Ratra-Peebles models, supernovae data put strong constraints on α which are tighten by cosmic shear, while for SUGRA models all observables are fairly insensitive to the value of this parameter. The corresponding constraints are given on Table 1.

trum; and their effective range extend to only about 1/5 of the top-hat variance one. Hence they follow more accurately the shape of the power spectrum at their measured range. For a power spectrum featureless at most scales but these, the independent measurements render this statistic the most convenient to use. In this case, contours from aperture mass variance are expected to be smaller than top-hat variance ones. But in general, the loss of information regarding the behaviour of models at other scales diminishes the capability of distinguishing between models. Consequently, the aperture mass variance contours are, in general, expected to be larger than top-hat variance ones. The difference is larger when analysing cosmic shear most important parameters. Since we are studying parameters to which cosmic shear is moderately sensitive to, the difference is not noticeable in our results of Fig. 8 and 9, but it is striking when using VIRMOS-Descart data to constrain the (σ_8, Ω_m) plane (van Waerbeke et al. 2001). Furthermore, for our data with measurements up to less than 1 deg, the largest power spectrum scale probed by the aperture mass variance is the one probed by the top-hat variance at around 10 arcmin and its full range effectively lies on non-linear scales, rendering its inferred parameters’ constraints less reliable, due to non-linear modeling uncertainties. For these two reasons, we will choose to use top-hat variance only, when producing the final results.

By using the full wide survey, we can try to disentangle the effects of the non-linear regime of structures formation by cutting off the small angular scales from the final analysis. In such a way, we can better investigate the distinction of cosmological parameters in the two classes discussed above, probing if dark energy primarily hangs on the background dynamics. The plots on the bottom line of Fig. 8 and 9 depict the analysis of the top-hat variance when taking into account only angu-

lar scales larger than 20 arcmin, corresponding to wavevectors $k \lesssim 1h \text{ Mpc}^{-1}$ at $z \lesssim \langle z \rangle / 2 \sim 0.5$, where therefore the effects of the non-linear regime are sub-dominant. The spread in the likelihood contours is more relevant for plots involving the primordial spectral index n_s , while the quintessence parameters (α, Ω_{Q0}) are not so much affected. Hence, one can study dark energy by cosmic shear using this technique even if not properly knowing how to deal with the non-linear regime. Obviously this conclusion has to be confirmed by a more complete study involving a larger parameter space, to account for other degeneracies.

The first line of Fig. 8 and 9 show the current results of CFHTLS-wide, using W1 and W3 data from an effective sky coverage of 22 deg². The corresponding marginalized constraints on α and Ω_{Q0} are a factor of 2 larger than the ones found with the synthetic data, depicted on the second line of the same figures. This is consistent with the reduction of the data error bars, which are proportional to $\sigma_e^2 n_{\text{gal}}^{-1} A^{-1/2}$, if cosmic variance is not taken into account. We must caution that the gain in the parameters space cannot be estimated with precision by this simple argument, namely by assuming

$$\text{gain} \sim \frac{r_{\sigma_e}^2}{r_{n_{\text{gal}}} \sqrt{r_A}}, \quad (31)$$

where the several factors r are the ratios between the features of the two surveys. In fact, the gain in the data error bars does not translate linearly into a gain in the parameters space confidence levels. That happens only in the Fisher matrix approximation, and even there, only in the case of statistical uncorrelated parameters. Furthermore, this reasoning does not take into account the extra constraining power coming from measurements at larger scales, as discussed earlier on, or simply

Table 1. Results of separate and joint analysis of cosmic-shear and Sn Ia data on quintessence parameters (α , Ω_{Q0}) at 68% (95%) confidence level. For Ratra-Peebles models, we quote only upper limits for α , the best-fit being always at $\alpha = 0$. Only for indicative purposes, we quote 68% confidence level limits on (w_{pivot} , w_a) parameters computed at $z_{\text{pivot}} = 0$, setting *n.c.* when not constrained. Remind that in this class of models $w_0 \geq -1$. See § 4.1 for discussion.

Ratra-Peebles					SUGRA				
	α	Ω_{Q0}	w_0	w_a		α	Ω_{Q0}	w_0	w_a
$\langle \gamma^2 \rangle$	< 14 (25)	$0.63^{+0.14(+0.15)}_{-0.17(-0.20)}$	n.c.	n.c.		$13^{+12(+12)}_{-5(-13)}$	$0.72^{+0.01(+0.03)}_{-0.02(-0.05)}$	$\lesssim -0.79$	$\gtrsim -0.45$
Sn Ia	< 1 (3)	$0.74^{+0.09(+0.16)}_{-0.10(-0.11)}$	$\lesssim -0.75$	$\gtrsim -0.13$		$12^{+5(+11)}_{-12(-12)}$	$0.77^{+0.04(+0.07)}_{-0.04(-0.08)}$	$\lesssim -0.84$	$\gtrsim -0.43$
$\langle \gamma^2 \rangle + \text{Sn Ia}$	< 1 (1)	$0.75^{+0.02(+0.03)}_{-0.04(-0.04)}$	$\lesssim -0.7$	$\gtrsim -0.13$		$2^{+7(+18)}_{-1(-2)}$	$0.74^{+0.03(+0.03)}_{-0.04(-0.05)}$	$\lesssim -0.84$	$\gtrsim -0.38$

coming from the fact of disposing of more degrees of freedom for the likelihood calculations.

It is also worthwhile to notice that, in all cases, (from Fig. 7 to Fig. 9), a Λ CDM model with a Harrison-Zel’dovich spectrum [$(\alpha, n_s) = (0, 1)$] is compatible with the data for $\Omega_{Q0} \sim 0.7$ at 99% confidence level.

4. Combining with other observables

4.1. Sn Ia

We combine the cosmic shear data by VIRMOS-Descart and CFHTLS-deep and -wide (22 deg² sub-sample) surveys with the type Ia supernovae “gold” set by Tonry et al. (2003). In particular, we evaluate confidence intervals considering cosmic shear and Sn Ia both separately and jointly. Indeed, since the distance modulus depends only on the background dynamics, we can restrict to the quintessence cosmological parameters α and Ω_{Q0} .

Figure 10 depicts both the independent and combined analysis for Ratra-Peebles and SUGRA models, using the top-hat variance data for the cosmic shear and computing the non-linear spectrum by the Peacock & Dodds (1996) mapping. The corresponding results are summarized in Table 1; these marginalized results for each parameter do not assume any prior knowledge of the other, apart from the flat priors implied by the range of the grid. Let us emphasize that the constraints obtained on (w_0 , w_a) inferred from those on the parameters of the potential differ when we change the form of the potential. This confirms that constraints on the equation of state derived from a general parameterization have to be interpreted with care.

Concerning Ratra-Peebles models, the weak lensing and Sn Ia contours are closer to mutual orthogonality, so narrow joint constraints are expected. Data strongly favor a quintessence component close to a cosmological constant, the best-fit lying always at $\alpha = 0$, hence in Table 1 we prefer to present the constraints as an upper limit. As it is clear from Fig. 10, Sn Ia are much more constraining for this parameter than weak lensing. However, even though Sn Ia alone reject $\alpha \geq 1$ at the 68% level, as was well known (Podariu & Ratra 2000), the information of weak lensing further narrows the interval.

As far as SUGRA models are concerned, for a wide interval of α (approximately $\alpha > 5$) both the luminosity distance and the shear two-point correlations are (almost) independent of this parameter, as it is clear from Fig. 10. In fact,

this conclusion was already reached studying the CMB temperature anisotropies (Brax et al. 2000), arguing that the equation of state does not strongly depends on the slope of the potential leaving both distances and linear growth factor almost unchanged. In terms of statistical significance, this means that the likelihood with respect to Sn Ia or weak lensing data alone is almost flat and so the best fit value has little meaning (see also Caresia, Matarrese & Moscardini 2004). In Table 1 we list the results in the form of a parameter value, which we take to be the likelihood weighted average of α , plus or minus the necessary deltas to form the confidence intervals obtained. However, for a substantial interval of α , weak lensing and Sn Ia lead to different, almost non-intersecting, ranges of Ω_{Q0} : Sn Ia favoring a higher value of Ω_{Q0} while weak lensing a lower one. Thus, even though both observables have limited sensitivity to constrain the parameter α , this fact allows to obtain a reasonable constraint from the joint likelihood, as that interval of α is rejected by the data. The joint confidence interval are substantially reduced, with a distinctive maximum of likelihood at $\alpha = 2$. Notice, however, that this is an unstable situation. In fact, if cosmic shear or supernovae contours slightly change their orientation and size, due for example to a larger uncertainty on the redshift of sources, the joint contour will easily degradate. On the contrary, the extreme situation, with both contours vertical and parallel for all α , would imply the abandon of the subjacent quintessence model. It has to be stressed that every systematic effect on weak-lensing or supernovae data as well, relying for instance on the data analysis procedure, strongly affects the final result; therefore special care is necessary when combining several datasets.

Provided that it is not evident which pivot redshift should be used when parameterizing these quintessence models by an equation of state of the form of Eq. (12), we superpose to the (Ω_{Q0} , α) plane, in Fig. (10), the contours for w_{pivot} and w_a corresponding to $z_{\text{pivot}} = 0$. Let us stress that the final results in terms of the equation of state parameters are only indicative. Interestingly, notice from Fig. 3 that for Ratra-Peebles models the estimation of w_{pivot} and w_a should not change if using $z_{\text{pivot}} = 0.5$ instead of $z_{\text{pivot}} = 0$. In fact, for this class of models, noticeably different values on these parameters only appear when considering a high pivot redshift. On the contrary, for SUGRA models the choice of the pivot redshift would be relevant already at low redshift. See Table 1 for specific constraints on w_0 and w_a .

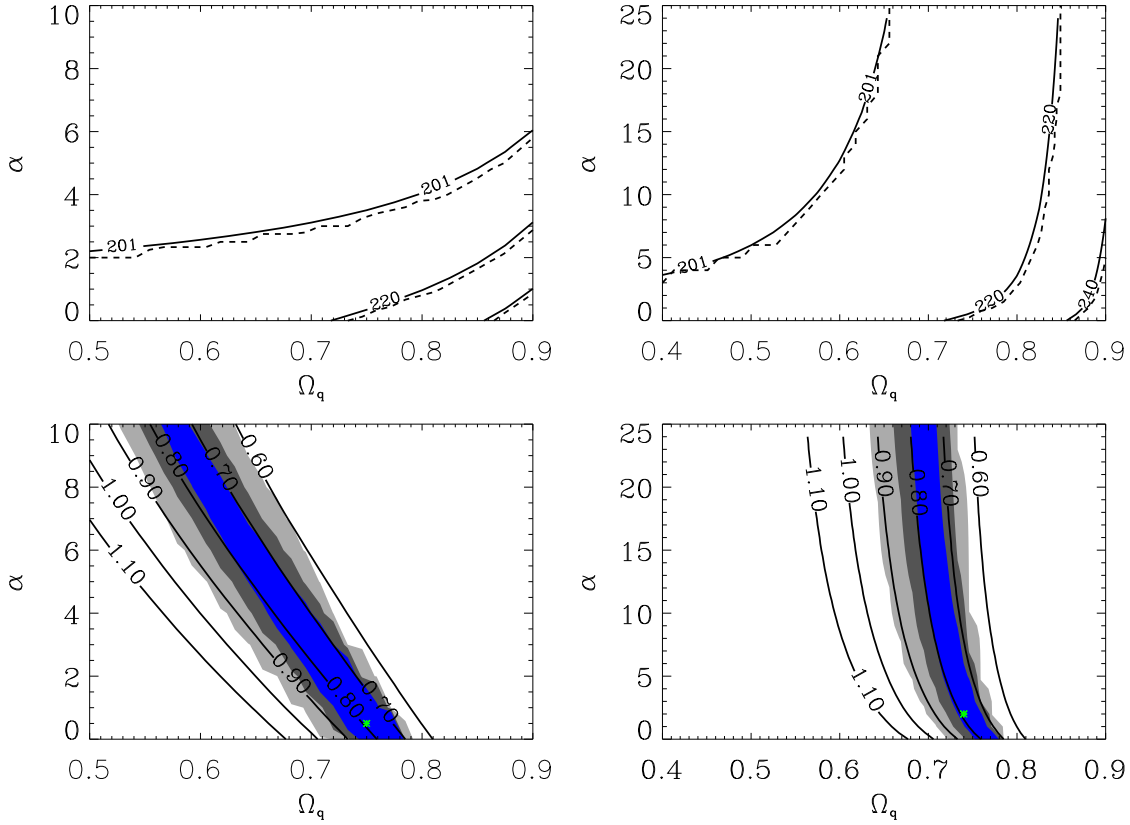


Fig. 11. Top line: Location of the first acoustic peak of the temperature CMB power spectrum, for Ratra-Peebles (left panel) and SUGRA (right panel) models. It is estimated using an analytical approximation lying on the solution of the background equations only (solid line), or by the full computation of C_ℓ s (dashed line). The central set of lines corresponds to the location of the first peak according to the best-fit of WMAP-1yr data, $\ell = 220.1 \pm 0.8$ (Page et al. 2003), while the left and right ones correspond to the multipoles $\ell = 201$ and $\ell = 240$, defining the smallest and the largest multipoles contributing to the three points of binned data defining the first peak (Hinshaw et al. 2003). Bottom line: Contour levels of σ_8 for Ratra-Peebles (left panel) and SUGRA (right panel) models with $n_s = 1$, superposed to the cosmic shear data contours (VIRMOS-Descart + CFHTLS-deep + CFHTLS-wide/22deg²). For indicative purposes, the star point marks the best-fit from the joint cosmic shear and SN Ia analysis, roughly sitting at $\sigma_8 = 0.8$. Remind that the spectrum was normalized on the CMB so this plots show the consistency with a normalization at $z = 0$. See § 4.2 for details.

Recently, weak lensing data (Semboloni et al. 2005; Hoekstra et al. 2005) were used to put constraints on w under the assumption it is a constant parameter. In that particular case, one has two characteristic redshifts, z_a and z_{de} , defining the beginning of the acceleration phase [$\ddot{a}(z_a) = 0$], and of the domination of the dark energy [$\Omega_m(z_{de}) = \Omega_{de}(z_{de})$]. They are given by

$$(1 + z_a)^{3w} = -\frac{1}{1 + 3w} \frac{\Omega_{de0}}{\Omega_{m0}}, \quad (1 + z_{de})^{3w} = \frac{\Omega_{de0}}{\Omega_{m0}} \quad (32)$$

so that $z_a > z_{de}$. When w becomes negative and large in absolute value, z_a and z_{de} tend to zero so that dark energy just starts almost today to dominate the universe and is redshifted in a way that it does not affect even low redshift observables. It follows that we expect the data to be insensitive to the value of w in that regime so that one can get only an upper limit on its value, as found by Semboloni et al. (2005) and Hoekstra et al. (2005). Indeed, such a situation cannot be achieved with a physical model as considered here because by construction it

imposes that $w > -1$. It follows that our approach is a physically motivated way of imposing a prior on w . Note also that Fig. 1 shows that $w = \text{constant}$ is not a good approximation of these two classes of models. At best the constraint on a constant w can be related to some redshift average of the equation of state. For these reasons, it is difficult to deduce a constraint on the physical models from a constraint on a constant w , even though the results of Table 1 are compatible with them.

4.2. CMB

CMB temperature anisotropies have been extensively used (see e.g. Baccigalupi et al. 2002; Jassal et al. 2004; Corasaniti et al. 2004) but several degeneracies amongst the cosmological parameters prevent to accurately constrain the cosmological parameters using CMB data only. Hence, concerning weak lensing, several studies already attempt to combine CMB and cosmic shear in order to constrain the

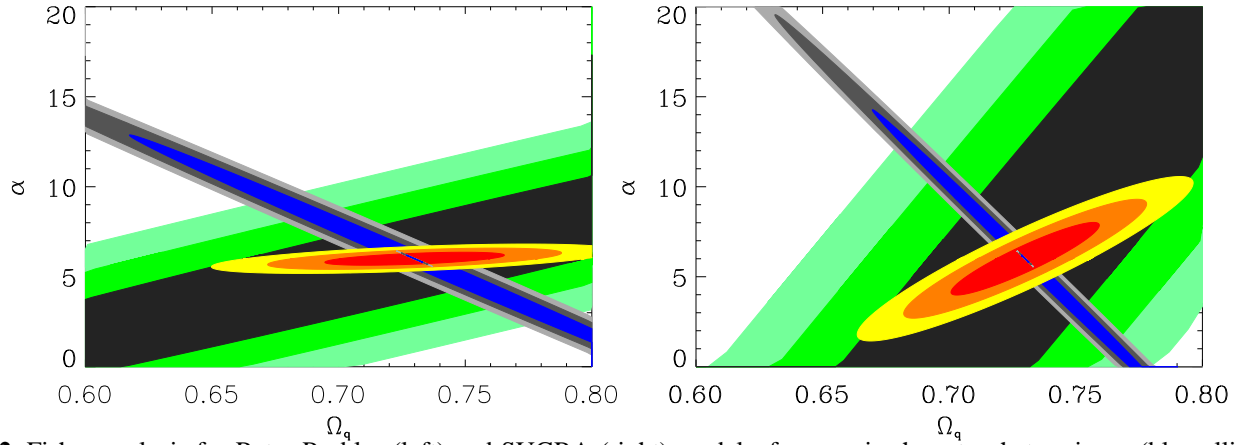


Fig. 12. Fisher analysis for Ratra-Peebles (left) and SUGRA (right) models, for cosmic shear top-hat variance (blue ellipses), Sn Ia “gold” set (green) and temperature CMB angular power spectrum by WMAP-1yr data (red) – contours at 68%, 95%, and 99% C.L. For the CMB, the noise matrix was computed using the public code by Verde et al. (2003). For cosmic shear, we consider both CFHTL-wide survey ($A = 170 \text{ deg}^2$, $n_{\text{gal}} = 20 \text{ gal/arcmin}^2$, $\sigma_e = 0.4$) and a space based survey ($A = 20,000 \text{ deg}^2$, $n_{\text{gal}} = 35 \text{ gal/arcmin}^2$, $\sigma_e = 0.3$), quoted as type II in the text. We consider only the quintessence parameters while the other parameters are kept *fixed*. See § 5 for discussion.

cosmological parameters (see e.g. Contaldi, Hoekstra & Lewis 2003; Ishak et al. 2004; Tereno et al. 2004).

As for dark energy, it affects the CMB anisotropies angular power spectrum at least in two ways (Brax et al. 2000). Firstly, the angular diameter distance is modified so that the peak structure is shifted. In particular the location of the first acoustic peak, depending on the geometry of the universe, provides an estimate of the angular diameter distance to the last scattering surface. However, also pre-recombination effects can shift the peaks from their true geometrical locations (Doran et al. 2000; Kamionkowski & Buchalter 2000). Secondly, the time evolution of the dark energy strongly affects the integrated Sachs-Wolfe effect. This effect is more relevant at low multipoles, modifying the amplitude of the spectrum, but it also leads to an additional shift of the Doppler peaks.

Beside using CMB data to normalize the power spectra (see § 3.4), we use them in still another way, by noticing that even without a statistical analysis of CMB data, we can strongly constrain cosmological parameters, and notably quintessence ones, simply by using the location of the first Doppler peak. Moreover, even without solving the perturbations equations and computing the TT spectrum, one can compute the acoustic scale just by solving the equation for the background evolution. The location of acoustic peaks is then estimated allowing for the shifts induced by the dark energy by means of a fitting formulae (Doran & Lilley 2002). In conclusion, the location of the first acoustic peak will be a function of the quintessence parameters (Ω_{Q0}, α), with a negligible dependence on the primordial spectral index n_s due to the shift correction. Using this analytic approximation, we individuate, in Fig. 10, the region of the (Ω_{Q0}, α) plane compatible with the location of the first acoustic peak of WMAP-1yr data (Hinshaw et al. 2003; Page et al. 2003) including the bins’ contributions to the three points defining the peak, namely $201 < \ell < 240$. Consistently with the normalization procedure we used, this result is in excellent agreement with that deduced by the complete computa-

tion of the TT spectrum, as shown in Fig. 11 (top panels). Let us notice that the region of the parameter space (Ω_{Q0}, α) compatible with the position of the first acoustic peak is degenerate with the Sn Ia constraints; the reason being that, since the pre-recombination effects of quintessence on the definition of the acoustic horizon at last scattering are negligible, the acoustic scale eventually depends only on the Hubble parameter like the luminosity distance, hence both are ultimately affected by quintessence approximatively in the same way.

As mentioned before, we may compute, a posteriori, the σ_8 value for each CMB normalized model. The obtained σ_8 iso-contours in the (Ω_{Q0}, α) plane are shown in Fig. 11 (bottom panels), setting $n_s = 1$. The σ_8 range that corresponds to the confidence levels found in this work, is in agreement with current cosmic shear σ_8 constraints; see Hoekstra et al. (2005) for a recent result and van Waerbeke & Mellier (2003) for a compilation of results. This shows the normalizations on the CMB and at $z = 0$ are compatible. It is interesting to note that the directions of the $\Omega_{Q0} - \alpha$ degeneracy for lensing data are lines of constant σ_8 . Being the curvature of the universe kept fixed, a strong constraint in σ_8 implies a strong constraint in Ω_{Q0} , through the well-known $\sigma_8 - \Omega_{m0}$ degeneracy, but only if Ω_{Q0} and α are not much correlated. This is what we observe in the SUGRA case. In general, a contour in the (σ_8, Ω_m) plane will move as a function of α and a strong constraint in σ_8 does not necessarily imply a strong constraint in Ω_{Q0} . This is what is obtained for the Ratra-Peebles case.

The computational tools we have developed (see Riazuelo & Uzan 2000; Schimd et al. 2005) allow us to compute, in the same framework, distance modulus, CMB anisotropies and weak lensing - cosmic shear effects. Hence, in principle there is no problem to combine Sn Ia and lensing data with CMB data. As already noticed, we have restricted here to a small parameter space. Indeed, a joint analysis with CMB data require a wider parameter space, possibly using the so-called “normal parameters” (see e.g. Sandvik et al. 2004),

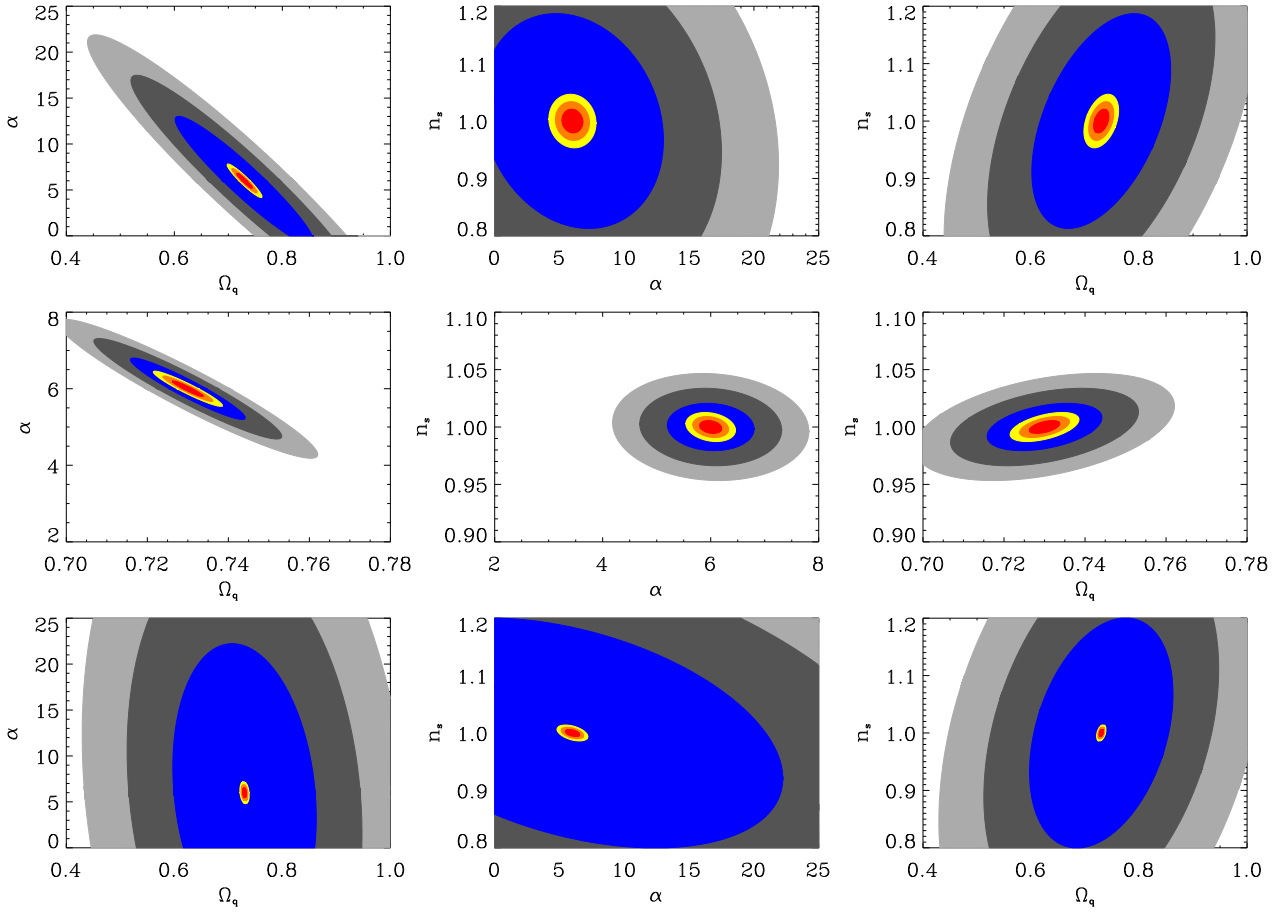


Fig. 13. Fisher analysis of weak lensing (top-hat variance) for Ratra-Peebles models, considering a CFHTLS-wide like survey and two space-based surveys layout (68, 95%, and 99% C.L.). Upper panels, analogous to the the likelihood analysis of Sec. 3 which also assumes all the other parameters fixed, compare a CFHTLS-wide like survey (wider ellipses) with a deep space-based survey with $A = 1,000 \text{ deg}^2$, $n_{\text{gal}} = 50 \text{ gal/arcmin}^2$, $\sigma_e = 0.3$. Middle panels compare the deep space-based survey with a wider but shallow space-based survey with $A = 20,000 \text{ deg}^2$, $n_{\text{gal}} = 35 \text{ gal/arcmin}^2$, $\sigma_e = 0.3$. Bottom panels compare the CFHTLS-wide like survey with the type I space-based survey, but marginalizing over τ_{reion} , left to vary. Compared with the first line, the last one shows the effect of a wider, more realistic parameters space. See § 5 for discussion.

an option left for a future study. In such a case, we would integrate our pipeline with a Markov chain Monte Carlo code (Tereno et al. 2005) developed for the likelihood analysis of cosmic shear. Furthermore, we will be able to include also the analysis of nucleosynthesis constraints, by means of a suitable code for quintessence models (Coc et al. 2006) which is able to deal with ordinary and extended quintessence models like the Boltzmann code and the lensing code used for this study.

5. Weak lensing: prospects on future data

Beyond CFHTLS, several next generation cosmic shear surveys are proposed in order to pin down w and the dark energy properties with exquisite details. It is interesting to explore the capabilities of such surveys to constrain the models discussed in this paper.

A comprehensive study of all projects and observing strategies is however beyond the scope of this work, so we deliberately focus on rather simple concepts where both sky coverage and depth are increased, assuming systematics related to shape

measurement can be discarded. In particular, we consider two possible layouts achievable by space-based missions. We will indicate by

- *type I*, a deep survey that would cover about $1,000 \text{ deg}^2$, one magnitude deeper than the CFHTLS-wide providing an effective galaxy number density around 50 gal/arcmin^2 ;
- *type II*, a wider but shallow survey, covering $20,000 \text{ deg}^2$ and yielding 35 gal/arcmin^2 .

Furthermore, we assume an intrinsic ellipticity distribution of galaxies similar to the one observed with current cosmic shear surveys with HST.

A Fisher analysis of Ratra-Peebles and SUGRA models, restricted to the parameters (Ω_{Q0}, α) keeping fixed the others, was performed around a fiducial model defined by $(\alpha, \Omega_{Q0}, n_s, h, \tau_{\text{reion}}, \Omega_{\text{baryon0}} h^2) = (6, 0.73, 1, 0.72, 0.17, 0.024)$. The results are presented in Fig. 12. Weak lensing surveys (blue ellipses) together with Sn Ia “gold” set (green ellipses) and CMB WMAP-1yr data (red ellipses) show that both quintessence parameters can in principle be determined with a

10% accuracy. The degeneracy with respect to Sn Ia and CMB would be almost totally broken. It is worth noticing that, since all cosmological parameters but the quintessence ones are kept fixed, we have to take with care the astonishing gain with respect to a CFHTLS-wide like survey (larger ellipses) achievable by a space mission of type II (smaller ellipses).

On scales larger than 10 degrees, the flat sky approximation used in § 3.1 does not hold anymore. Indeed, an angular distance of 15 degrees on a sphere has a 1% deviation from the same distance on a plane, and for larger scales spherical harmonics must be considered (Stebbins 1996). These effects are not taken into account in the results of Fig. 12, where the gain observed between the two weak lensing ellipses essentially corresponds to Eq. (29), together with contributions from the fact that measurements from two surveys observing at different scale ranges have different cosmic variances and different degrees of freedom when fitting models to the data. In particular, a strategy of dividing the covered surveys areas in patches of 100 deg^2 is assumed. Hence, given the large ratio between both sky coverages, this is the dominant factor in the gain.

For indicative purposes, and allowing for the effect of systematic discussed in § 4.1, we restrict the Fisher analysis of weak lensing (top-hat variance) to Ratra-Peebles models, considering a CFHTLS-wide like survey and both the space-based surveys of type I and type II; see Fig. 13. As in § 4.1, we evaluate the parameters space $(\alpha, \Omega_{Q0}, n_s)$. In the upper line, analogous to the likelihood analysis of Sec. 3, which also assumes all the other cosmological parameters fixed, we compare the CFHTLS-wide like survey (wider ellipses) with the space-based surveys of type I (smaller ellipses). The middle line is analogue, but comparing space-based surveys of type I (wider ellipses) with the space-based surveys of type II (smaller ellipses); notice that the apparent rotation of the ellipses is simply due to a rescaling of the axes. As for quintessence parameters, a space-based survey of type II gives 99% C.L. contours approximately 3 times smaller than those achievable by a type I survey. Indeed more cosmological parameters have to be taken into account. As an example, allowing the reionization optical depth τ_{reion} to vary, the likelihood contours get strongly modified; see the third line of Fig. 13, where we compare a CFHTLS-wide like and type II space-based surveys, marginalizing over τ_{reion} . They get larger and the degeneracies directions are changed. The strong impact of the reionization optical depth in cosmic shear results comes from the degeneracy with between τ_{reion} and the normalization of the spectrum.

The great predictive power of space-based surveys will allow to simultaneously constrain a large number of parameters with a good precision, even if not so high as the one showed in the analysis of a small number of parameters. However, it is important to notice that we have not taken into account the possible use of tomography based on a decomposition of lensing data into several lensed/source planes, nor any use of higher order statistics than the top-hat shear variance. So, even if several issues have been neglected in the present study, our conclusions are likely not over-optimistic.

6. Conclusions

In this article, we have investigated the constraints set by weak lensing, supernovae and CMB data on two families of quintessence models.

In such a situation where a physical model is fully specified, we can treat both the background and perturbation evolution without any ambiguity, in particular when dealing with high redshift data. Such an approach is thus complementary, as discussed in Section 2, to those based on a parameterization of the dark energy sector, in particular when trying to infer constraints on a physical model from those on the parameters of the equation of state. This also enables to get rid of the pivot redshift problem when combining different data sets. From a more theoretical point of view, such models cannot lead to an equation of state $w < -1$, contrary to an arbitrary parameterization. It is thus interesting to determine whether there is a tension in the data when such a physical constraint is imposed, as would be concluded from various studies indicating that $w < -1$ is favored.

To achieve this task, we have used a set of numerical tools that allow to compute background, CMB and lensing signatures of a large class of cosmological models including quintessence and some extensions such as scalar-tensor theories. We have focused our analysis on three cosmological parameters, the index of the primordial power spectrum and two parameters describing the quintessence models, along with an extra-parameter for the sources distribution (see § 3.4). Although one can criticize such a small parameter space, it is sufficient to give an idea of the parameter space available for quintessence models and to discuss how weak lensing data can improve the constraint on dark energy. This choice was also driven by numerical limitations but our analysis will be extended to a larger set of parameters in a near future.

We have normalized the initial power spectrum to the CMB so that σ_8 is now a prediction of the models and is not used for normalization. Note also that we do not require to specify an analytical form for the transfer function. Weak lensing predictions are also sensitive to the linear to non-linear mapping and we have discussed the effect of such mapping on the constraints with care. In particular, we have shown that, while the parameters of the primordial spectrum are sensitive, those of the dark energy sector remain robust. We have also tested the possibility to cut the weak lensing data sets (such as the CFHTLS-wide) in order to reduce the influence of the non-linear regime.

This analysis is the first one using CFHTLS data to study the dark energy and illustrates the complementarity of these observations with other data sets. To finish, we have also forecast how space-based wide field imagers will improve our knowledge of dark energy. In particular, we have considered two possible strategies, the first deeper and the second wider but shallower. The latter turns out to be more suited to track dark energy as far as cosmic shear is concerned. The constraints on the two classes of quintessence models considered in this article are shown on Fig. 10 and Table 1. They can be summarized as follows: For a flat universe and a quintessence inverse power law potential with slope α , we get $\alpha < 1$ and $\Omega_{Q0} = 0.75^{+0.03}_{-0.04}$.

at 95% confidence level, whereas $\alpha = 2^{+18}_{-2}$, $\Omega_{Q0} = 0.74^{+0.03}_{-0.05}$ when including supergravity corrections.

In the future, we plan to improve this analysis by first comparing it to a similar analysis based on a parameterization of the equation of state, by enlarging the parameter space, by addressing more carefully the problem of the redshift distribution of galaxies and by shifting from a grid method to an MCMC method.

Acknowledgements. We thank Nabila Aghanim, Karim Benabed, Francis Bernardeau, Daniel Eisenstein, Bernard Fort, Simon Prunet, Alexandre Réfrégier and Jim Rich. CS acknowledges “Fondazione Angelo Della Riccia” and “Fondazione Ing. Aldo Gini” for financial support. IT is partly funded by the CNRS/ANR research grant “ECOSSTAT”, contract number ANR-05-BLAN-0283-04. LF thanks the “European Association for Research in Astronomy” training site (EARA) and the European Community for the Marie Curie doctoral fellowship MEST-CT-2004-504604. LVW, HH are supported by the Natural Sciences and Engineering Research Council (NSERC), the Canadian Institute for Advanced Research (CIAR) and the Canadian Foundation for Innovation (CFI). We thank the CNRS-INSU and the French Programme National de Cosmologie for their support to the CFHTLS cosmic shear program.

References

- Amendola, L. 2000, Phys. Rev. D, 62, 043511.
- Athreya, R., et al. 2002, A&A, 384, 743.
- Baccigalupi, C., et al. 2002, Phys. Rev. D, 65, 063520.
- Bacon, D., Réfrégier, A., & Ellis, R. 2000, MNRAS, 318, 625.
- Bartelmann, M., & Schneider, P. 2001, Phys. Rep., 340, 291.
- Benabed, K., & Bernardeau, F. 2001, Phys. Rev. D, 64, 083501.
- Benabed, K., & van Waerbeke, L. 2003, Phys. Rev. D, 67, 123515.
- Basset, B. A., et al. 2002, MNRAS, 336, 1217.
- Basset, B. A., Corasaniti, P. S., & Kunz, M. 2004, Phys. Rev. D, 69, 083517.
- Bennett, C. L., et al. 2003, ApJS, 148, 1.
- Brax, P., & Martin, J. 1999, Phys. Lett. B, 468, 40.
- Brax, P., Martin, J., & Riazuelo, A. 2000, Phys. Rev. D, 62, 103505.
- Caldwell, R. R., & Linder, E. V. 2005, Phys. Rev. Lett., 95, 141301.
- Caresia, P., Matarrese, S., & Moscardini, L. 2004, ApJ, 605, 21.
- Carroll, S. M. 2001, Living Rev. Rel., 4, 1.
- Chevallier, M., & Polarski, D. 2001, Int. J. Mod. Phys. D, 10, 213.
- Chiba, T. 1999, Phys. Rev. D, 60, 083508.
- Coc, A., et al. 2006 [astro-ph/0601299].
- Contaldi, C., Hoekstra, H., & Lewis, A. 2003, Phys. Rev. Lett., 90, 221.
- Corasaniti, P. S., & Copeland, E. J. 2003, Phys. Rev. D, 67, 063521.
- Corasaniti, P. S., et al. 2004, Phys. Rev. D, 70, 083006.
- Crocce, M., & Scoccimarro, R. 2005 [astro-ph/0509418 and astro-ph/0509419].
- Dave, R., Caldwell, R. R., & Steinhardt, P. J. 2002, Phys. Rev. D, 66, 023516.
- Dolag, K., et al. 2003, A&A, 416, 853.
- Doran, M., et al. 2001, ApJ, 559, 501.
- Doran, M., et al. 2001, Phys. Rev. D, 64, 123520.
- Doran, M., & Lilley, M. 2002, MNRAS, 330, 965.
- Hamilton, A. J., et al. 1991, ApJ, 374, L1.
- Hinshaw, G., et al. 2003, ApJS, 148, 135.
- Hoekstra, H. 2003, IAU Symposium 216, *Maps of the Cosmos*, ASP Conference Series, eds. M. Colless & L. Staveley-Smith, Sydney, July 2003 [astro-ph/0310908].
- Hoekstra, H., et al. 2005, accepted by ApJ[astro-ph/0511089].
- Hu, W., & Jain, B. 2004, Phys. Rev. D, 70, 043009.
- Hu, W., & White, M. 1997, Phys. Rev. D, 56, 596.
- Huterer, D., & Takada, M. 2005, Astropart. Phys., 23, 369.
- Ishak, M., Hirata, C., McDonald, P., & Seljak, U. 2004, Phys. Rev. D, 69, 083514.
- Jarvis, M., Jain, B., Bernstein, G., & Dolney, D. 2005, accepted by ApJ[astro-ph/0502243].
- Jassal, H. K., Bagla, J. S., & Padmanabhan, T. 2004, MNRAS, 356, L11.
- Jain, B., & Taylor, A. 2003, Phys. Rev. Lett., 91, 141302.
- Jing, Y. P., et al. 2005 [astro-ph/0512426].
- Kaiser, N., Wilson, G., & Luppino, G. 2000 [astro-ph/0003338].
- Kamionkowski, M., & Buchalter, A. 2000 [astro-ph/0001045].
- Klypin, A., et al. 2003, ApJ, 599, 31.
- Kujat, J., et al. 2002, ApJ, 572, 1.
- Linder, E. V., 2003, Phys. Rev. Lett., 90, 091301.
- Linder, E. V., & Huterer, D., 2005, Phys. Rev. D, 72, 043509.
- Ma, C. P., & Fry, J. N. 2000, ApJ, 543, 503.
- Ma, C. P., et al. 1999, ApJ, 521, L1.
- Mainini, A., et al. 2003, ApJ, 599, 24.
- Martin, J., Schmid, C., & Uzan, J.-P., 2006, Phys. Rev. Lett., 96, 061303.
- McCracken, H. J., et al. 2003, A&A, 410, 17.
- McDonald, P., Trac, H., & Contaldi, C. 2006, MNRAS, 366, 547.
- Mellier, Y. 1999, ARA&A, 37, 127.
- Padmanabhan, T., 2003, Phys. Rep., 380, 235.
- Page, L., et al. 2003, ApJS, 148, 233.
- Peacock, J. A., & Dodds, S. J. 1996, MNRAS, 280, L19.
- Peebles, P. J. E. 1993, Principles of physical cosmology (Princeton University Press).
- Peebles P. J. E., & Ratra, B. 2003, Rev. Mod. Phys. 75, 559.
- Peter, P., & Uzan, J.-P. 2005, Cosmologie primordiale (Belin).
- Podariu, S., & Ratra, B. 2000, ApJ, 532, 109.
- Ratra, B., & Peebles, P. J. E. 1988, Phys. Rev. D, 37, 3406.
- Refregier, A. 2003, ARA&A, 41, 645.
- Riazuelo, A., & Uzan, J.-P. 2000, Phys. Rev. D, 62, 083506.
- Riazuelo, A., & Uzan, J.-P. 2002, Phys. Rev. D, 66, 023525.
- Riess, A. G., et al. 2004, ApJ, 607, 665.
- Sachs, R. K. 1962, Proc. Roy. Soc. A, 270, 103.
- Sandvik, H. B., et al. 2004, Phys. Rev. D, 69, 063005.
- Scherrer, R.J. 2005 [astro-ph/0509890].
- Schimd, C., Uzan, J.-P., & Riazuelo, A. 2005, Phys. Rev. D, 71, 083512.
- Schneider, P., Ehlers, J., & Falco, E. E. 1992, Gravitational lenses (Springer.)
- Schneider, P., van Waerbeke, L., Kilbinger, M., & Mellier, Y. 2002, A&A, 396, 1.
- Seljak, U. 2000, MNRAS, 318, 203.
- Semboloni, E., et al. 2005 [astro-ph/0511090].
- Simpson, F., & Bridle, S. 2005, Phys. Rev. D, 71, 083501.
- Smith, R. E., et al. 2003, MNRAS, 341, 1311.
- Spergel, D. N., et al. 2003, ApJS, 594, 1.
- Stebbins, A., 1996, [astro-ph/9609149].
- Tereno, I., et al. 2005, A&A, 429, 383.
- Uzan, J.-P. 1999, Phys. Rev. D, 59, 123510.
- Uzan, J.-P., 2004, AIP Conference Proceedings 736, *Phi in the Sky: The Quest of Cosmological Scalar Fields* [astro-ph/0409424].
- Uzan, J.-P., & Bernardeau, F. 2000, Phys. Rev. D, 63, 023004.
- Uzan, J.-P., & Bernardeau, F. 2001, Phys. Rev. D, 64, 083004.
- Uzan, J.-P., Aghanim, N., & Mellier, Y. 2004, Phys. Rev. D, 70, 083533.
- van Waerbeke, L., & Mellier, Y. 2003, Lecture given at the Aussois winter school, France, January 2003 [astro-ph/0305089].

- van Waerbeke, L., Mellier, Y., Erben, T., et al. 2000, A&A, 358, 30.
- van Waerbeke, L., Mellier, Y., Radovich, M., et al. 2001, A&A, 374, 757.
- van Waerbeke, L., Mellier, Y., & Hoekstra, H. 2005, A&A, 429, 75.
- van Waerbeke, L., et al. 2006, in preparation.
- Verde, L., et al. 2003, ApJS, 148, 195.
- Wetterich, C. 1988, Nucl. Phys. B, 302, 668.
- Wittman, D. M., et al. 2000, Nature, 405, 143.
- Yahata, N., et al. 2000, ApJ, 538, 493.
- Zhan, H., & Knox, L. 2004, ApJ, 616, L75.